Using Human Induced Pluripotent Stem Cell Derived Cardiomyocytes as a Model for Catecholaminergic Polymorphic Ventricular Tachycardia: Visualizing Calcium Handling

by

Kevin Ye

B.Sc. (Hons.), University of British Columbia, 2017

Thesis Submitted in Partial Fulfillment of the
Requirements for the Degree of
Master of Science

in the
Department of Biomedical Physiology and Kinesiology
Faculty of Science

SIMON FRASER UNIVERSITY

Fall 2022

Declaration of Committee

Name:	**Kevin Ye**
Degree:	**Master of Science (Biomedical Physiology and Kinesiology)**
Title:	**Using Human Induced Pluripotent Stem Cell Derived Cardiomyocytes as a Model for Catecholaminergic Polymorphic Ventricular Tachycardia: Visualizing Calcium Handling**
Committee:	**Chair:** **Charles Krieger** Professor, Biomedical Physiology and Kinesiology **Glen Tibbits** Supervisor Professor, Biomedical Physiology and Kinesiology **Damon Poburko** Committee Member Associate Professor, Biomedical Physiology and Kinesiology **Zachary Laksman** Committee Member Assistant Professor, Medicine University of British Columbia **Thomas Claydon** Examiner Professor, Biomedical Physiology and Kinesiology

Abstract

Cardiovascular diseases are one of the leading causes of death in the developed world. Human induced pluripotent stem cell derived cardiomyocytes are a relatively novel model for studying cardiovascular diseases that have the advantage of being of human origin over conventional animal models. Calcium handling is an important aspect in causing diseases such as catecholaminergic polymorphic ventricular tachycardia (CPVT), therefore monitoring Ca2+ kinetics within the cardiomyocytes is an important aspect for studying those diseases. This project proposes the design and use of a genetically encoded calcium indicator, R-CEPIA1$_{SR}$, in combination with traditional calcium sensitive dyes in order to monitor both the cytosolic and sarcoplasmic reticulum luminal calcium levels simultaneously. The optogenetic constructs BLINK2 and Phobos can further help control the cell for easier observation of Ca2+ events. This will lead to a better understanding of the mechanisms behind CPVT related variants and eventually lead to better treatments in combating them.

Keywords: Optogenetics; Genetically Encoded Calcium Indicators; Induced Pluripotent Stem Cells; Cardiomyocytes

Acknowledgements

I would like to thank my senior supervisor Dr. Glen Tibbits for all his patience, support, and wisdom throughout the years and putting up with all my great jokes while somehow managing to keep a straight face. I am incredibly lucky to have been a part of his lab and have learned so much over my time here.

Thank you to my committee members Dr. Damon Poburko and Zachary Laksman for agreeing to be on my committee and providing feedback on my thesis. Thank you to Dr. Tom Claydon for agreeing to be my external examiner and to Dr. Charles Krieger for chairing it.

A special thanks to all of our collaborators without whom this project would have been much more difficult. Thank you to Dr. Anna Moroni for her knowledge and help with our BLINK2 construct, Dr. Francis Lynn and his lab for his support and expertise in CRISPRing our construct, Dr. Leif Hove-Madsen for creating and guiding me on how to use his calcium analysis software, Dr. Wayne Chen and his student Mads Søndergaard for their help with organelle entrapped calcium indicators, and Dr. Ziwei Ding for his support and expertise in cloning.

Thank you to all the lab members past and present for your support and guidance. Especially to Shayan who created the filtering program used to de-noise my files. Every day was always interesting thanks to you all.

Finally a special thank you to my parents for all their love and support.

Table of Contents

List of Tables

List of Figures

Introduction

Induced pluripotent stem cells and their derived cardiomyocytes

The heart is a critical organ that has notoriously low regenerative capacity[1]. Cardiovascular disease (CVD) is one of the leading causes of death in developed countries. In the USA alone, 49% of adults >20 years of age suffer from CVD at some stage of their lives and costs the economy ~$378 billion each year[2]. Given the prevalence and severity of CVDs, it is imperative to find more effective treatments to counteract the problem. Primary cardiomyocytes (CMs) have a tendency to quickly dedifferentiate in culture, losing sarcomeres, mitochondria, and electrical coupling[3] over a short period of time. Due to these problems, research involving CMs traditionally required harvesting them fresh from animal models such as mice. However, the applicability of animal model results to humans is challenging as there are some significant differences between human and animal models. Nevertheless the process of drug development relies heavily on animal models to identify potential new molecules based on their efficacy and toxicity in the preclinical stage[4]. Unfortunately the translation of drugs from animals to humans has a high attrition rate, typically hovering at around 90%[5,6], with the leading cause being lack of efficacy or unexpected toxicity in humans (the metrics that were identified in animal models)[5,7]. A renewable source of human cells such as human embryonic stem cells can be a potential alternative to animal primary CMs and the problems they come with. However, they also come with many ethical considerations and are mired in controversy. In 2006, future Nobel laureate Shinya Yamanaka discovered four factors (Oct3/4, Sox2, c-Myc, Klf4) that could induce pluripotency in adult differentiated fibroblasts[8]. These cells would be called human induced pluripotent stem cells (hiPSCs). The application of this discovery can produce a nearly endlessly replenishable supply of pluripotent stem cells that can be obtained from any human donor at any time, while being free from the ethical controversies surrounding human embryonic stem cells. Methods to differentiate these cells into specific lineages, including CMs, were then developed allowing a renewable supply of human CMs to be used in research. This particular method of sourcing CMs also has another advantage in that it maintains the donor's entire genetic background. Genetically inherited diseases, such as catecholaminergic polymorphic ventricular tachycardia

(CPVT), can be caused by variants in specific genes that alter their function leading to the disease phenotype. It is well documented that that multiple people can be harboring the same variant suspected of causing the disease, yet are affected to vastly different degrees; for some the phenotype can be debilitating or lethal while others may appear asymptomatic[9]. As hiPSCs can be derived from individuals known to be afflicted by the disease in question, and harbor the rest of the patient's genetic background, accounting for any potential effects the background would have on the penetrance of the variant of interest. Furthermore, through the usage of powerful genetic editing tools such as the CRISPR/Cas9 system, one can reverse the variant of interest and create an isogenic control or introduce the variant to a healthy patient's genome.

hiPSC-CMs are attracting attention as a powerful new tool that can be used to model a variety of diseases, and the effects of drugs for the treatment of those diseases, or any other potential side effects. The Comprehensive in vitro Proarrhythmia Assay (CiPA) consortium is an initiative to establish a new paradigm for the screening of drugs. This new method seeks to use hiPSC-CMs as a model combined with data from patch clamping and *in silico* modelling for testing the arrhythmic potential of drugs. Traditional methods for screening any drug, no matter its intended usage, involve assaying for its activity on I_{Kr} generated by the channel encoded by human ether-a-go-go-related gene (hERG). Prior to this screening requirement, some commercially available drugs such as the antihistamine drug Terfenadine had hERG blocking activity. hERG is responsible for the rapid component of the delayed rectifying potassium current (I_{KR}) and blockers can potentially cause QT interval prolongation, early after depolarizations (EADs), Torsades de Pointes (TdP), and potentially sudden cardiac death[10]. Drugs that can block I_{KR} began receiving attention when some individuals taking them exhibited sudden cardiac arrest[11,12]. This led to a wide range of drugs being withdrawn from the market over safety concerns after the discovery of their hERG blocking potential, including antimalarials, antibiotics, antihistamines, and ironically antiarrhythmics[11] due to their affecting the QT interval and potentially leading to sudden death. Pharmaceutical companies have since then been required by the FDA to show their drugs had no hERG blocking activity for safety approval; however, this condition may have been a bit overzealous. Drugs such as Verapamil have shown hERG blocking activity without affecting the QT interval due to its ability to also block calcium channels having a compensatory effect and are still in use due to being approved prior to 2005 when ICH E-14 came into effect, and a lack of

arrhythmogenic consequences allowing it to be recognized as safe. Among the many drugs that have been abandoned due to hERG blocking activity, it could include drugs that have compensatory effects and would thus be safe to use. The unwarranted loss of these potentially useful drugs can be avoided through the use of hiPSC-CMs as a better model to more accurately capture the effects of drugs on the human heart rather than simply looking at a single ion channel in isolation.

The main downside of using hiPSC-CMs as a model are mainly due to their immaturity. Instead of an adult-like phenotype, hiPSC-CMs exhibit a more fetal-like form with less organized sarcomeres, differences in ion channels that retain automaticity (automatic spontaneous beating), reliance on glycolysis instead of fatty acid based metabolism, and lack of T-tubules[13,14]. Differences in ion channel expression especially are particularly important in the context of using these cells as a model for adult diseases in electrophysiology. As a consequence, the subject of maturing hiPSC-CMs so that they exhibit a more adult-like phenotype is a very active field that in the future could remove these shortcomings entirely[14–17]. Nevertheless, hiPSC-CMs still remain an excellent standard for drug testing and disease modelling as maturation protocols are rapidly improving.

Excitation contraction coupling

Ca^{2+} is an important and versatile ion acting as a messenger in a wide variety of cell signalling pathways[18]. In the context of excitation contraction coupling (ECC), Ca^{2+} is used as both a signal to release more Ca^{2+} from the sarcoplasmic reticulum (SR), and to bind to troponin in order to initiate muscle contraction.

The SR is a specialized organelle found in myocytes that acts as a store for Ca^{2+}. Through proteins such as Calsequestrin (CASQ) which buffers free calcium and sequesters it away in long polymers[19], and SarcoEndoplasmic Reticulum Calcium ATPase (SERCA) to move calcium from the cytosol into the SR against its concentration gradient, the SR can reach free Ca^{2+} levels in the mM range during diastole, and hundreds of μM during systole[20], while total Ca^{2+} levels (including those bound in CASQ) can reach as high as 20 mM[19].

This large store of Ca^{2+} is controlled by and released back into the cytosol through ryanodine receptors (RyR). RyRs are very large ion channels that localize to the SR membrane as tetramers, and have 3 different paralogs: RyR1 is found mainly in skeletal muscles, RyR2 in cardiac, and RyR3 in the brain, although they can also be found to varying degrees in other tissues[21]. These channels themselves are capable of detecting Ca^{2+} levels and a high enough local concentration can induce their opening and result in the release of more Ca^{2+}, eventually causing a global Ca^{2+} transient in a process called calcium induced calcium release (CICR). RyR2s are normally organized into clusters of calcium release units (CRUs), and grouped with other proteins important for their function, such as the voltage gated calcium channel $Ca_V1.2$. This voltage gated channel connects to the extracellular space through T-tubules, allowing the entry of Ca^{2+} into the cytosol when activated and increasing the local Ca^{2+} concentration in the dyadic space, resulting in CICR. RyR2s are also capable of detecting Ca^{2+} on the SR lumen side, and if it gets to a sufficiently high concentration, would also cause RyR2 to open in a process called store overload induced calcium release (SOICR)[22], and has been identified as a possible mechanism for adventitious Ca^{2+} release in diseases[23–25].

RyR2 can open stochastically without triggering through $Ca_V1.2$ and release small puffs of Ca^{2+} referred to as Ca^{2+} sparks. This process does not release enough Ca^{2+} to cause a global calcium transient through CICR but rather results in being limited in both time and space[26]. Sparks are important as they provide a method of regulating SR Ca^{2+} levels[27] and their characteristics, such as frequency or duration, can be used as an indicator of abnormalities in Ca^{2+} handling and RyR2 itself[28,29]. Due to the important role of RyR2 in Ca^{2+} handling, genetic variants of RyR2 are often associated with cardiac diseases such as CPVT.

The primary method of extracellular Ca^{2+} entry into CMs is through the L-type calcium channel $Ca_V1.2$, a voltage gated calcium channel that begins to open at -35 mV[30,31]. Normal resting membrane potential for native adult human CMs is at -80 mV, therefore $Ca_V1.2$ normally stays closed during diastole. On the other hand, hiPSC-CMs have a resting membrane potential of around -60 mV[14], which while still not at the activation threshold for $Ca_V1.2$, is very close to the activation threshold for the voltage gated sodium channel $Na_V1.5$, which is at -55 mV, the activation of which would lead to an action potential throughout the cell, and activating $Ca_V1.2$. At this level of resting V_m, it is likely that a higher percentage of $Na_V1.5$ channels are in an inactive state compared

to a normal Vm of -85 to -90 mV, and are unable to respond to depolarization[32,33]. This contributes to the hiPSC-CM's property of spontaneous beating, a property that adult primary CMs do not have, which can interfere with measurements requiring quiescent cells. $Ca_V1.2$ brings in about 30% of the total Ca^{2+} during a contraction cycle, while most of the rest is released from the SR[34]. The combined Ca^{2+} increase from extracellular and SR sources then bind to cardiac troponin C (cTnC encoded by TNNC1), causing a conformational change in cTnC and then in the entire tropomyosin complex on the thin filament. This exposes myosin binding sites on the actin which allows the creation of cross bridges between the thick and thin filaments and resulting in a contraction (Figure 1). The movement arising from contraction during imaging can interfere with precise recordings. Therefore, the contraction must be decoupled from the excitation, typically through drugs such as blebbistatin or mavacamten.

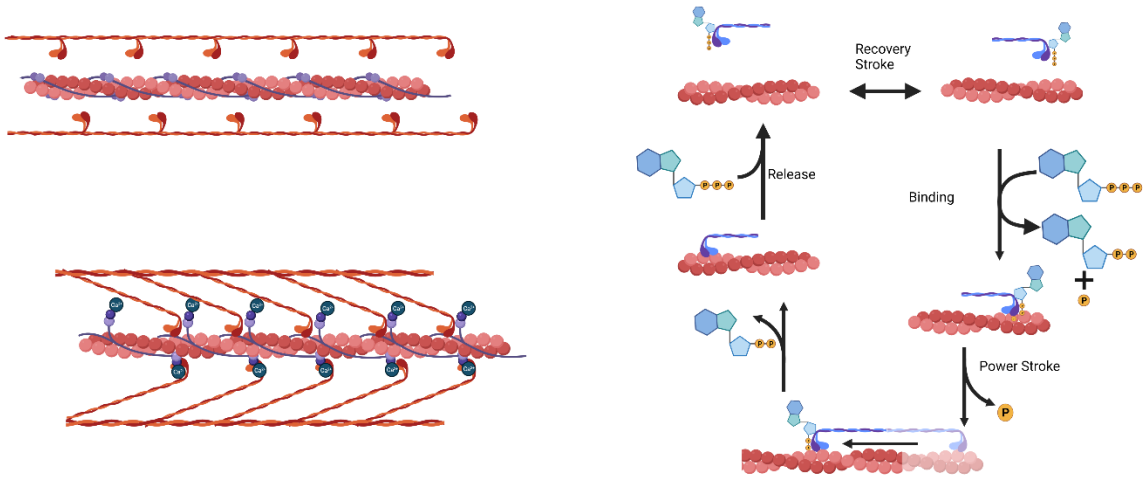

Figure 1: Muscle contraction process in presence of Ca^{2+}.
Left: Increased cytosolic Ca^{2+} levels cause shifting of troponin exposing myosin binding sites.
Right: Process of myosin binding to actin, forming cross bridges, and pulling to generate force.

Catecholaminergic Polymorphic Ventricular Tachycardia

Catecholaminergic polymorphic ventricular tachycardia (CPVT) is a potentially lethal inheritable cardiac arrhythmia. Under normal conditions, the disease could be imperceptible as the affected go about their lives but can be suddenly triggered to potentially lethal terms by physical or emotional stress by activating the β-adrenergic receptors (βARs). The genetic variants that trigger CPVT typically do not affect cardiac structure and combined with a lack of abnormalities in resting ECG, make it a particularly difficult disease to detect, and the first diagnosis of the disease in the family is often done after cardiac arrest. As the disease is inheritable, the remaining family members can then be properly diagnosed via genetic testing and stress tests in a controlled environment. βAR stimulation from stress can trigger premature ventricular complexes (PVCs) in patients which can be detected through ECGs, and if no measures are taken, can eventually develop into polymorphic and/or bidirectional ventricular tachycardia.

Genetically, the majority of CPVT cases can be traced back to variants in RyR2 and are collectively known as CPVT1. Other proteins involved in the handling of Ca^{2+}, either directly or through downstream effects, have also been implicated in the genetic cause of CPVT and have their own variant of CPVT (Table 1). In CPVT1, most mutations in RyR2 are gain-of-function (GoF) mutations; variants that result in RyR2 opening more often and/or at lower concentrations of Ca^{2+}.

Table 1: Types of CPVT and their prevalence

Type of CPVT	Causal Gene	Protein	Prevalence in CPVT
CPVT1	RyR2	Cardiac Ryanodine Receptor	60-65%
CPVT2	CASQ2	Calsequestrin 2	2-5%[35]
CPVT3	TECRL	Trans-2,3-enoyl-CoA Reductase-like	<1%[36]
CPVT4	CaM1	Calmodulin 1	<1%
CPVT5	TRDN	Triadin	<1%

Molecularly, the effects of GoF variants in RyR2 include mutations that destabilize the interaction between subunits either by being located directly in the interaction sites or causing conformational changes from a longer range resulting in a more open conformation even while closed[37], variants that affect the interactions with regulatory proteins or phosphorylation sites resulting in a lack of regulation[38], mutations directly in the pore forming region affecting Ca^{2+} permeation[39], and mutations affecting

the folding of RyR2 itself[40]. These variants all have the effect of increasing leakage of Ca^{2+} from the SR, usually in the form of sparks, waves, or wavelets, although other sources such as reverse mode SERCA are also known to contribute a sizeable amount[41].

The resulting Ca^{2+} leakage from the SR raises cytosolic Ca^{2+} levels, causing an overactive sodium calcium exchanger (NCX), which exchanges a single Ca^{2+} for 3 Na^{+} ions – a net positive charge difference. This charge can contribute to prolonging the AP or even triggering another depolarization, causing a delayed after depolarization (DAD) and lead to ventricular tachycardia.

βAR stimulation is important to support the movement of a greater volume of blood in the heart in response to stress. This involves faster SR Ca^{2+} loading to maintain a higher level of Ca^{2+} for greater contraction strength (inotropy), and increased off kinetics for Ca^{2+} of contractile machinery to increase the speed of relaxation (lusitropy) due to decreased troponin affinity for Ca^{2+} in order to shorten the time necessary for a contraction cycle in order to allow a faster heart rate (chronotropy)[42–46]. This allows for overall faster and greater contractility in order to pump the greater volume of blood necessary for the expected increase in physical exertion. In the case of hiPSC-CMs, β-adrenergic stimulation can be triggered with βAR-agonists, such as isoproterenol, to simulate conditions under which an affected cell line is expected to result in CPVT[47]. βAR act through the secondary messenger cyclic AMP (cAMP) to activate protein kinase A (PKA), which goes on to phosphorylate downstream proteins[45]. Among them is phospholamban (PLB) which is an inhibitor of SERCA when dephosphorylated, but reversed when phosphorylated[48]. SERCA then becomes more active, increasing the speed of reloading SR Ca^{2+} levels as well as the amount, allowing for increased contraction force at a faster heart rate[42,48]. As well, phosphorylation of $Ca_V1.2$ by PKA and Ca^{2+}/Calmodulin-dependent protein kinase II (CaMKII) increases the amount of Ca^{2+} passing through $Ca_V1.2$ from outside the cell, increasing the overall Ca^{2+} available inside the cell[30]. In addition, phosphorylation of RyR2 increases its open probability leading to a greater Ca^{2+} leak through RyR2. PKA phosphorylates RyR2 at Ser2808, but CaMKII also phosphorylates RyR2 at Ser2808 and Ser2814[49], and some claim that CaMKII is more relevant for the CPVT phenotype than PKA, while also having the capability to be upregulated by βAR stimulation due to the increased $[Ca^{2+}]$[46,49,50]. This increased open

probability in turn also leads to an increased Ca^{2+} leak rate from the SR in the form of sparks.

In addition to leakage from the SR, RyR2s can detect SR luminal Ca^{2+} levels and will open if that rises above its threshold. The threshold for spontaneous opening of RyR2 channels in healthy CMs is still higher than the increased SR Ca^{2+} levels during β-adrenergic stimulation, so this increase does not have clinical consequences. Some variants of RyR2 can increase their sensitivity to SR luminal Ca^{2+} levels, lowering the threshold required for opening. This altered threshold is still higher than normal resting SR luminal Ca^{2+} levels, making them near undetectable in that state, however the increased SR Ca^{2+} levels from β-adrenergic stimulation can surpass the altered RyR2 threshold, leading to the opening of RyR2 and causing Store Overload Induced Calcium Release (SOICR). This mechanism has been proposed as an important mechanism for CPVT[51]. CPVT related RyR2 variants have previously been generated and expressed in HEK293 cells (using the ER as a Ca^{2+} store) by the Chen group at the University of Calgary. Even without voltage-dependent channels to trigger RyR2 on the cytosolic side due to being HEK cells, increasing amounts of Ca^{2+} on the ER luminal side ($[Ca^{2+}]_{ER}$) resulted in RyR2 spontaneously and consistently opening when $[Ca^{2+}]_{ER}$ reached a certain point. Through the use of D1ER, a FRET based ER luminal Ca^{2+} indicator, to visualize $[Ca^{2+}]_{ER}$, they were able to track the minimum and maximum range of $[Ca^{2+}]_{ER}$ and the $[Ca^{2+}]_{ER}$ relative to that at which each RyR2 variant would spontaneously open (Figure 2)[52]. In addition, in direct measurements of a single RyR2 channel embedded in a planar lipid bilayer between two reservoirs, the open probability of RyR2 showed similar levels at low Ca^{2+} levels on the luminal side, while at higher luminal Ca^{2+} levels CPVT related variants had higher open probability than WT (Figure 3)[22]. Overall, these experiments provide strong mechanistic evidence of RyR2's ability to respond to luminal Ca^{2+} levels, and how CPVT related RyR2 variants would alter that. However, these experiments were performed with RyR2 in isolation, lacking much of the sophisticated Ca^{2+} handling machinery found in CMs. Whether through an increased $[Ca^{2+}]_{SR}$ or increased open probability of RyR2, β-adrenergic stimulation leads to Ca^{2+} leak into the cytosol from the SR resulting in DADs.

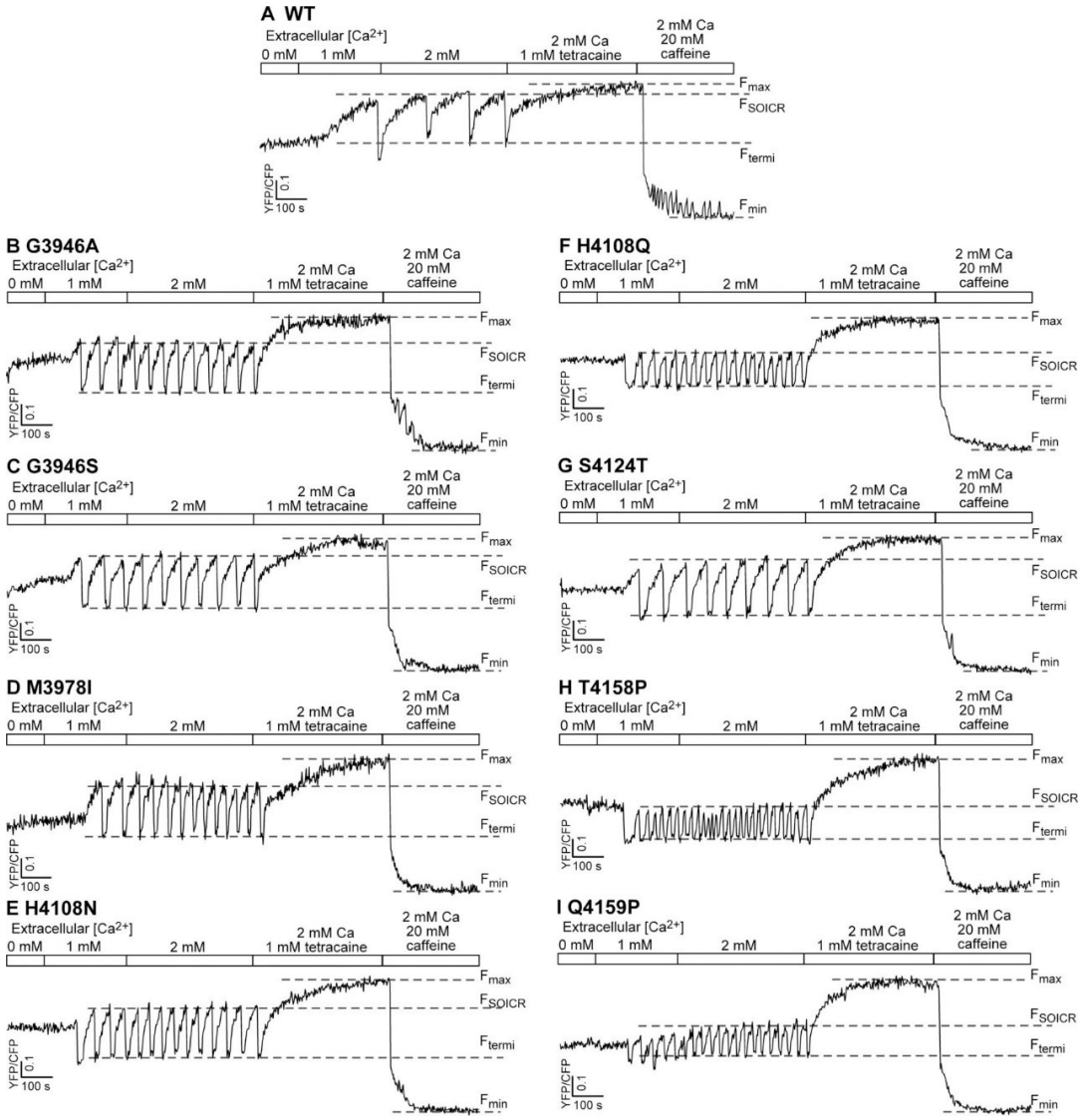

Figure 2: Luminal ER Ca^{2+} measurements in HEK293 cells

HEK293 cells expressing RyR2 variants showing varying levels of endoplasmic reticulum (ER) luminal Ca^{2+} at which RyR2 will open based on the variant. A greater distance between F_{SOICR} and F_{max} indicates a lower $[Ca^{2+}]_{SR}$ threshold at which opening occurs. The fluorescent indicator is FRET based D1ER. Image adapted from Xiao et al. 2016[52]

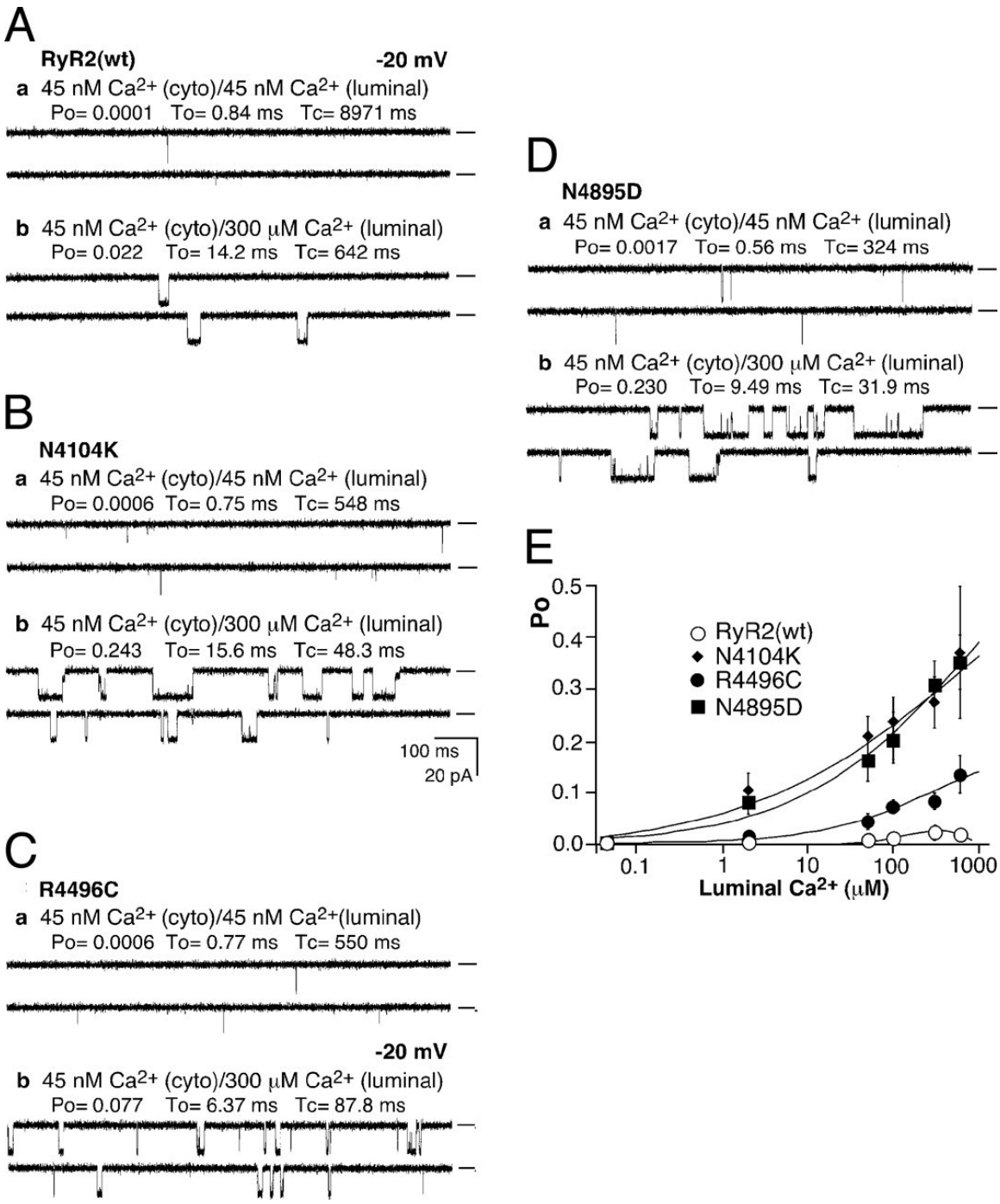

Figure 3: Open probabilities of a singular RyR2 channel embedded in a planar lipid bilayer.

Open probabilities for CPVT related RyR2 variants are similar at low "luminal" Ca^{2+} while CPVT variants are much higher at higher Ca^{2+} levels. Image adapted from Jiang et al. 2004[22].

Clinical treatment is typically done pharmacologically through βAR blockers, or calcium-channel blockers which are used as an adjunct in addition to beta-blockers, or as a replacement for patients who are unable to take beta-blockers[25]. Although the exact mechanisms are not known, blocking of beta adrenergic stimulation is effective due to the basis of triggering CPVT being through βAR stimulation[25,53], while Ca^{2+} channel blockade is thought to help return the higher cytosolic Ca^{2+} levels that comes with its mishandling back closer to normal levels[54]. Patients shown to be refractory to βAR blockers are also commonly treated with Flecainide, a Na^{+} channel and RyR2 blocker, in addition as an adjuvant to some success[55]. Pharmacological intervention is adequate for ~70% of CPVT patients[36], however patients who are unresponsive to pharmacological treatment must be treated through more invasive methods. Such patients may have to undergo surgical denervation[56] or rely on implantable cardiac defibrillators (ICD), but these are not ideal as they are very invasive and come with their own set of problems[54]. Thus, it is important to identify the efficacy of treatments as soon as possible and find new alternatives for those who do not respond to current existing drugs.

Genetically Encoded Calcium Indicators

Being able to observe and image Ca^{2+} is an important requirement for tracking the effects that a variant or drug may have on Ca^{2+} handling. There are already a wide variety of small molecule dyes capable of entering into live cells and emitting fluorescence in the presence of Ca^{2+} (e.g., fura-2, fluo 4, Rhod-2). However, these molecules are not easily targetable to specific organelles, and also have a toxic effect on the cells affecting long-term cell viability, as well as leaking out of the cells over time. Genetically encoded calcium indicators (GECI) are a method of visualizing Ca^{2+} through the use of genetically encoded proteins to both detect Ca^{2+} and emit fluorescence. In this method there is limited toxicity to the cell, allowing for measurements over multiple time points or longitudinal studies[57]. This is particularly useful when there is a long time period over which a treatment's effects are expected to manifest or are otherwise not readily apparent immediately. Small molecule fluorescent indicators do have advantages such as higher response speed, greater color variety, increased dynamic range, and overall better fluorescence signal, however newer GECIs are being developed to improve on these properties[58].

Most GECIs follow a similar design as the early CaMP GECIs, namely they have a calmodulin domain to detect Ca^{2+}, an RS20 or M13 peptide fragment from smooth muscle light-chain kinase for CaM to bind to when activated, and one or two chromophores in between them[59]. Two chromophore systems typically are Forster resonance energy transfer (FRET) based, where bringing one constitutively excited chromophore near the other one will excite that one and are particularly useful as a ratiometric indicator for measuring an absolute value for [Ca^{2+}]. Single chromophores are generally reliant on the conformational change of CaM binding to M13, altering the chromophore so that it is able to absorb energy and become excited[59]. Unfortunately, fluorescent proteins are normally based on the GFP structure and thereby designed as β barrel structures surrounding the chromophore responsible for fluorescence, protecting it from outside forces. The 5' and 3' ends of a fluorescent protein are usually located close together in the final folded form but towards the outside of the structure, so any conformational changes applied after connecting those ends with the rest of the GECI are absorbed by the β barrel, and do not result in large changes on the essential chromophore[60]. Therefore, fluorescent proteins used for GECIs are often circularly permuted (cp) to expose the chromophore to the effects of conformational changes brought about by the rest of the GECI. By connecting the canonical ends together with a linker of peptides and creating a new break elsewhere that will become the new 5' and 3' ends, the fluorescent protein's connections to the GECI can therefore be made anywhere on the fluorescent protein, including adjacent to the chromophore[61] (Figure 4). However finding the appropriate locations to circularly permute a fluorescent protein can be a very labourious and tedious process, and often results in problems such as decreased brightness, and increased sensitivity to environmental effects such as pH, and in the case of mApple, a photoswitching property[60,62]. Photoswitching is a phenomenon whereby the excitation of a protein induces a conformational change. In the context of mApple, this causes it to change to a form that cannot be excited by its typical excitation wavelength, and thus temporarily loses its ability to fluoresce, leading to a fluorescence drop of ~50% in a population[63,64]. This is a reversible process and mApple has been shown to revert back to its rest state after being left in darkness[63]. Due to the difficulty in producing new cp fluorescent protein variants, there are few good options in the red spectral range available to use in GECIs, although it is still an ever evolving field[62,65].

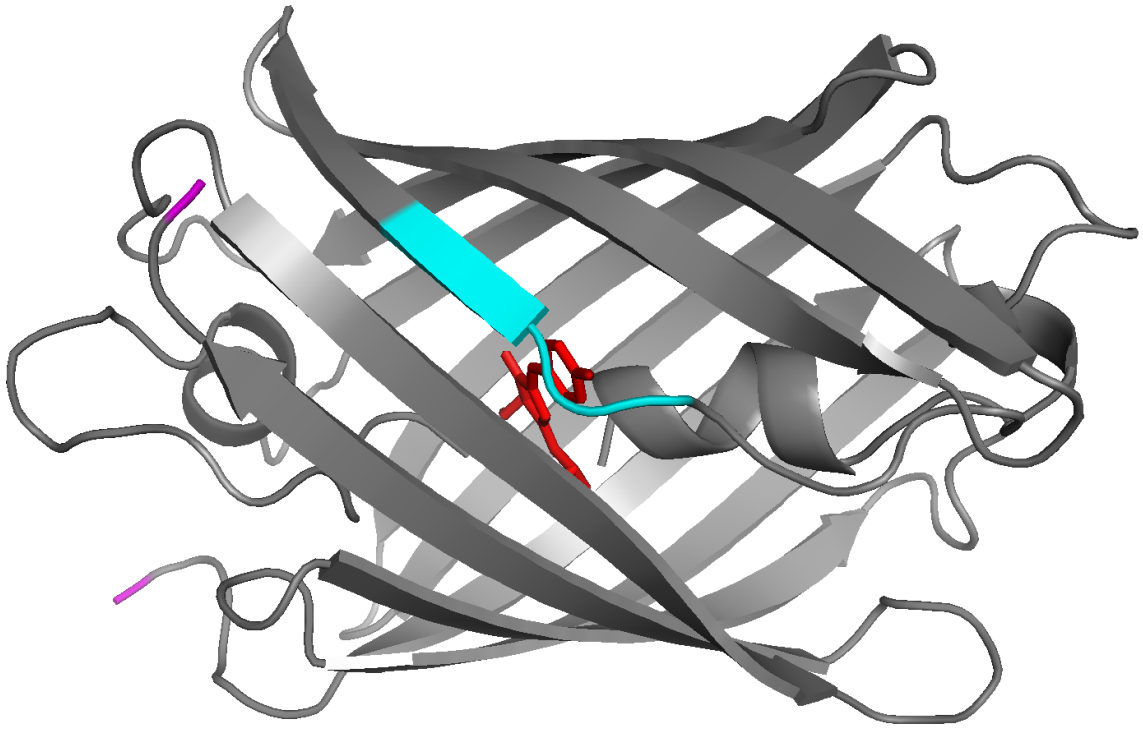

Figure 4: Cartoon of a typical fluorescent protein.
The red chromophore is protected by a barrel of beta-sheets, attenuating any external forces applied through the purple canonical ends of the protein. Circular permutation joins the purple ends together with a linker and places a new cut at the teal area creating new ends. Forces applied at the teal location located closer to the red chromophore result in greater changes allowing adjustment of fluorescence levels.

Methods to localize small molecule dyes to organelles do exist, and involve loading the entire cell with lower affinity dyes and attempting to accumulate the dyes in the organelles using esterases, in a method called targeted esterase induced dye loading (TED). However this method does not actively target the dyes to the organelles and a large portion is still left in the cytoplasm, as well as being limited only to areas whereby there are high concentrations of esterases[66,67]. GECIs and other genetically encoded indicators on the other hand can be specifically targeted not only to the ER, but any other organelle or desired location in the cell through the application of localization signals attached to the protein.

Triadin Red Calcium-measuring Organelle-entrapped Protein Indicator 1 in the SR (TRDN-R-CEPIA1$_{SR}$) is one such GECI that is useful for measuring Ca^{2+} levels in the SR. It consists of the classic GCaMP style design, but with the fluorescent protein replaced with mApple for a red signal, the calmodulin mutated to reduce Ca^{2+} affinity, and triadin attached to help localize it to the SR. Through R-CEPIA1$_{SR}$, direct

measurement of SR Ca^{2+} levels are made possible, allowing visualization of SR Ca^{2+} levels during caffeine application to observe the degree of SR Ca2+ depletion, RyR inhibition to observe the maximum SR load, or inhibition of SERCA to determine the SR Ca^{2+} leak rate. This in turn allows better quantification of SOICR and various factors that contribute to it.

Optogenetics

Optogenetics is the usage of light to control a protein function, and thus the cell function. The archetypical example of optogenetic proteins are rhodopsins[68]. Rhodopsins consist of opsin, a 7-transmembrane domain protein, coupled to retinal, a chromophore that detects light and causes a change in the opsin protein. Depending on the type of opsin, the mechanism of action for affecting cell function can be through ion channels and pumps (type I) or through G-protein pathways (type II)[69]. Methods to control ion movement are particularly useful for studying CMs as it allows one to control membrane potential without needing to patch clamp the cell. This means it is possible to pace the cells, or alternatively silence the cells through exposure to light of the appropriate wavelength. In contrast to native adult CMs, hiPSC-CMs have a more fetal-like phenotype; one aspect of this is that they are typically beating spontaneously without requiring external voltage changes. This results in a constant background of global Ca^{2+} transients, which can interfere with the detection of smaller Ca^{2+} releases such as sparks as they can be drowned out by the transients, or otherwise affect the sparks due to the constant cycling of SR Ca^{2+} levels.

Light-activated ion pumps are capable of moving ions against their electrochemical gradient allowing more control, however as they are pumping against that gradient, they also require energy in order to function. Running these pumps therefore, can start to affect ATP/ADP ratio levels and electrochemical gradients across membranes, causing other unintended side effects[70]. In addition, ion channel-based rhodopsins only require photons to open the channel initially to allow a large number of ions through, while ion pumps require at least 1 photon for each cycle of the pump, and thus require greater light intensity and duration than ion channels to achieve the same effect[71,72].

One critical reason for the spontaneous transients in hiPSC-CMs is the low expression of K^+ channels, specifically the inward rectifying K^+ channels Kir2.1 and Kir2.2. Typically these channels would normally bring the resting membrane potential (RMP) of CMs closer to the equilibrium potential of K^+ at ~-85 mV[73], but due to a lower expression of these channels in immature hiPSC-CMs, their resting membrane potential is more depolarized[10]. In patch clamp experiments, simulating the addition of this I_{K1} back has been shown to be capable of disabling the automaticity[74]. Expressing channels to decrease RMP, ideally one that can generate a current similar to I_{K1} and be controlled, is therefore expected to disable the automaticity of the hiPSC-CMs.

BLINK2 is an optogenetic K^+ channel that responds to blue light (<500 nm)[75]. It combines a 94 amino acid tetrameric K^+ channel from chlorovirus (Kcv)[76] with a blue light responsive photoreceptor from *Arabidopsis* (LOV2), utilizing flavin mononucleotide (FMN) as its chromophore[77]. The maximum absorbance of the FMN is 447 nm, which upon exposure will undergo a reversible change to bond cysteine in its active form, and then revert back to its inactive form in the dark[78]. When expressed in hiPSC-CMs, BLINK2 is expected to compensate for the low expression of K^+ channels when activated, allowing V_m to move down towards E_K, thus hyperpolarizing the hiPSC-CMs.

Alternatively, the inverse can also accomplish the same goal of cessation of spontaneous beating. Voltage gated channels open once reaching their threshold voltage, and then inactivate after reaching a high enough membrane voltage and are unable to open again until they recover at a hyperpolarized membrane potential. By depolarizing the cells instead of hyperpolarizing them, voltage gated channels will be prevented from recovering by holding them in the inactivated state and thus also prevent them from activating.

Phobos is a blue light (467 nm) activated optogenetic Cl^- channel developed as a more blue-shifted anion-conducting channelrhodopsin, and has previously been shown to inhibit action potentials in the neurons of *Drosophila* larvae *in vivo*[79]. Cl^- has an equilibrium potential of ~-50 mV in CMs[80] and will leave the cell down its electrochemical gradient at rest; Phobos activation will therefore depolarize the cell and hold the cell at a membrane potential close to -50 mV, preventing any further depolarisations from occurring. However, this method is less preferable to BLINK2 as increasing K^+ currents is more physiologically relevant.

By preventing voltage gated ion channels from opening, either through holding them below their activation potential or preventing them from recovering, it is expected to result in the cessation of spontaneous action potentials in the hiPSC-CMs, allowing the measurement of sparks.

Lentivirus

Lentivirus is a retrovirus that randomly integrates into the host genome and is commonly used as a vector for gene transfer in animal cells, and has even been considered as a candidate for gene therapy in patients[81]. Originally based on Human Immunodeficiency Virus (HIV-1), lentiviruses being used as a vector have been modified to remove their ability to reproduce so that they can only undergo a single round of infection. 2nd generation and 3rd generation lentiviruses have undergone further modification to improve their safety compared to the initial vectors and are still commonly used today. The 2nd generation of lentivirus has the genome split into a transfer plasmid, which contains the actual genetic information that will be contained in the virus, and two support plasmids for packaging and envelope production necessary for formation of the virus itself. There is still a small risk that can occur due to recombination of those 3 plasmids; if the packaging and envelope genes were to recombine into the transfer plasmid, replication competent lentivirus can still be produced. The 3rd generation lentivirus further improves the safety by splitting the envelope plasmid into two separate plasmids, for a total of 4 different plasmids (transfer, pkg, rev, env) that require recombination to make a replication competent lentivirus. The plasmids are transfected into a packaging cell line such as HEK293 cells in order to produce the lentivirus, which are then collected for later transduction into the relevant cells. Upon infection of a cell, lentivirus will randomly integrate into the host's genome resulting in a long-term and stable expression in even non-dividing cells like CMs[82].

CRISPR/Cas9

The Clustered Regularly Interspaced Short Palindromic Repeats (CRISPR) Cas9 nuclease system has been a transformative method to genetically edit living organisms. Discovered as a bacterial defense mechanism used to defend itself against phage infections via nuclease activity, it has since been repurposed to cut DNA at specific sites

at which researchers wish to introduce a change via single guide RNAs. A double strand break in the DNA is only a small point of concern for the cell as there exist mechanisms for repairing such damage. Non-homologous end joining (NHEJ) is one of two such mechanisms that commonly occurs during a CRISPR Cas9 edit; it involves taking the ends of a double stranded break and directly attaching them together. This process is fairly error-prone and can lead to indels causing frameshift mutations which, although often acceptable if the end goal is to simply knock out the gene in question, is not a preferred outcome when precision editing is needed to replace a nucleotide or insert a sequence in frame. The other common repair mechanism is known as homology directed repair (HDR). In HDR, a template that matches the damaged area has to be provided in order to repair the cut. This would normally revert the cut DNA back to its original form when the cell uses its own genome as the template. However, if exogenous DNA that matches the area except for a small mutation happens to be present, that DNA may be used as the template instead and the repaired DNA will then carry that new mutation. Through this method, the CRISPR/Cas9 system is capable of using the cell's own DNA repair mechanism to introduce mutations, insertions, or deletions at a specific point of interest *in vivo*.

Genomic safe harbour sites

Genomic safe harbour sites are areas in the genome that are stable enough to allow the insertion of a large sequence of DNA without impacting the cell in any noticeable way, while being robust enough for long term consistent expression of the inserted gene. Using genome editing tools such as CRISPR/Cas9, a transgene can be controllably introduced *in vivo* to a genomic safe harbour site without evidently impacting any of the organism's functions. The most commonly used genomic safe harbour site in humans is the Adeno-Associated Virus integration Site 1 (AAVS1) locus, located in the first intron of the Protein Phosphatase 1 Regulatory Subunit 12C (PPP1R12C) gene[83]. Originally discovered as a hotspot for adeno-associated virus (AAV) to preferably integrate its DNA into[84], scientists have emulated AAVs and turned them into hotspots for their transgene integration as well. Prior to the advent of powerful genomic editing tools, AAV's relatively predictable integration was one of few alternatives to the random integration of retroviruses for introducing a new gene *in vivo,* which was especially important for procedures such as gene therapy[85,86]. This history coupled with a lack of

noticeable deleterious effects have led to its popularity as a hotspot for integration even now in the era of CRISPR/Cas9[87,88]. Unfortunately, the locus may not be an appropriate genomic safe harbour site in all circumstances; some studies have shown that in the case of hiPSCs, promoter silencing in AAVS1 can occur. Thus an alternative site would be preferable for transgene insertion in hiPSCs[89]. A second intronic region of Citrate Lyase Beta-Like (CLYBL) site, originally discovered as an integration hotspot for PhiC31 recombinase, has been proposed as an alternative to AAVS1. It has been shown to not only improve on the issues of AAVS1 in hiPSCs, but has > 10 times higher transgene expression[90]. Therefore, we will attempt to insert our transgenes BLINK2 and R-CEPIA1$_{SR}$ into the CLYBL locus rather than AAVS1.

Objectives

Ca^{2+} handling is a critical component of CPVT pathology, and the SR as the main store for Ca^{2+} in CMs. Abnormalities in Ca^{2+} handling can be reflected in changes in $[Ca^{2+}]_{SR}$ load and increased leakage can result in the CPVT phenotype. Therefore, being able to track $[Ca^{2+}]_{SR}$ levels will be very helpful in determining the mechanisms through which specific variants cause CPVT and provide a target for improved treatments and diagnostics of the disease. The purpose of this project is the creation of a system to be used for the monitoring of SR Ca^{2+} levels and sparks in hiPSC-CMs in order to investigate CPVT mechanisms. To this end, the constructs R-CEPIA1$_{SR}$ and BLINK2 will be integrated into hiPSC-CMs, to visualize SR Ca^{2+} levels, through the CRISPR/Cas9 system into a genomic safe harbour site, or through lentiviral transduction. This will be followed up by validating the constructs' expression and function through imaging live hiPSC-CMs. As well, if necessary for R-CEPIA1$_{SR}$, making adjustments to improve the distinctiveness of each signal, maximizing the SR reporter (through adjusting imaging methods or improving expression levels) and minimizing overlap between the different reporters. The end goal will be a hiPSC-CM based platform capable of detecting both cytosolic and SR Ca^{2+} levels and adjustable quiescence on demand (Figure 5).

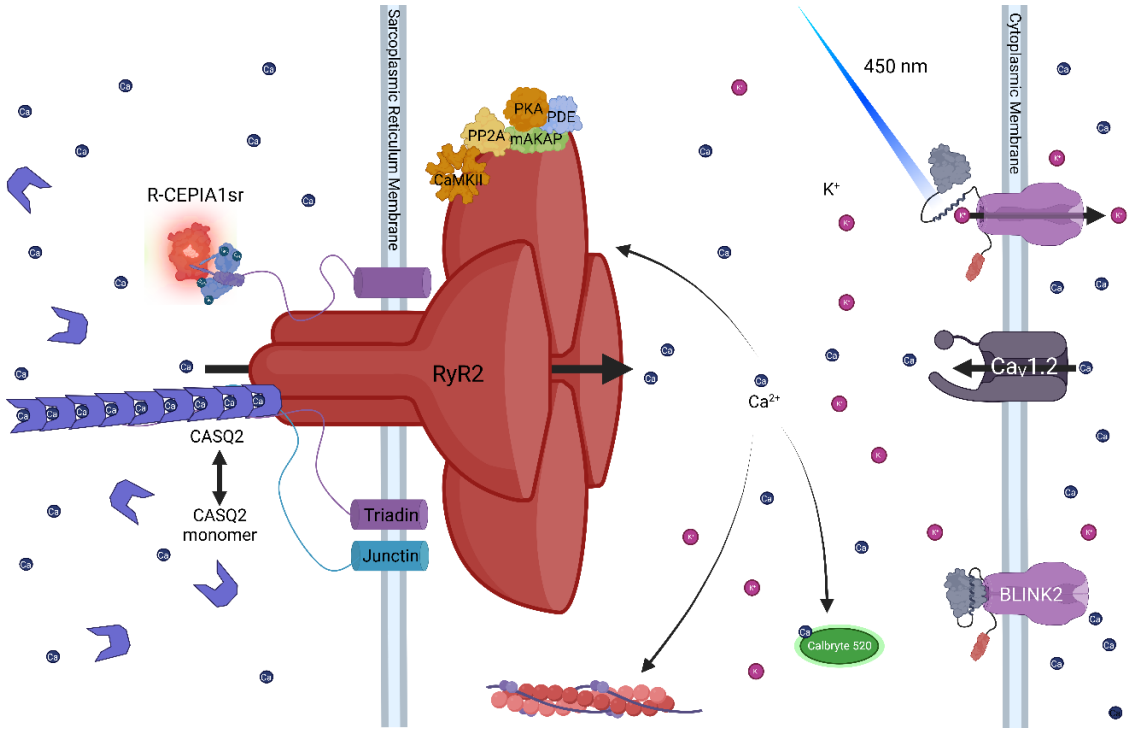

Figure 5: Proposed platform for visualizing Ca^{2+} handling in CMs.
R-CEPIA1$_{SR}$ detects free Ca^{2+} in the lumen of the sarcoplasmic reticulum (SR) and fluoresces based on the concentration. Calsequestrin (CASQ2) binds free Ca^{2+} and forms polymers to store it. Triadin and Junctin are SR membrane proteins and help mediate interactions between CASQ2 and RyR2, Triadin is also attached to R-CEPIA1$_{SR}$ for localization. RyR2 has many regulators such as Calmodulin Dependent Protein Kinase II (CaMKII), Phosphokinase A (PKA), muscle-specific A-kinase anchoring protein (mAKAP), protein phosphatase 2 (PP2A), and phosphodiesterase (PDE). RyR2 is activated by cytosolic Ca^{2+} coming through the voltage gated calcium channel Ca$_V$1.2 during depolarization, which can be prevented by activation of the light activated K^+ channel BLINK2.

Methods

hiPSCs and maintenance

Human induced pluripotent stem cells were obtained commercially from WiCell Research Institute (Madison, WI). Maintenance of the hiPSCs was done in a standard 6 well plate and followed a daily media change of mTeSR Plus media (StemCell Technologies Catalogue #: 100-0276) until cells reached a confluency of ~70%. Cells that reach confluency were split 1/15 into a new well coated in Matrigel or Geltrex extracellular matrices. To detach cells, cells were washed in PBS followed by ReLeSR, and then incubated dry at 37 °C for 6 minutes. After incubation, cells were readily detached with addition of mTeSR media, and broken down to small clumps of 2-5 cells before being passaged into the new well. Freshly passaged cells had their media supplemented with 10 μM of the ROCK inhibitor Y-27632 (StemCell Technologies Catalogue #: 72302).

hiPSC-CM differentiation and maintenance

To differentiate hiPSCs to CMs, hiPSCs were seeded at a density of 250,000 cells/well in a 6 well plate at single cell clump sizes. Differentiation largely followed the protocol by Lian et al.[91] for Gsk3 inhibition which in turn activates Wnt followed by Wnt inhibition. In brief, cells were allowed to grow following standard hiPSC maintenance for 3 days until reaching a confluency of at least 50%, upon which would be day 0 of the differentiation procedure. Media were then changed to RPMI basal media with 2% B27 supplement without insulin with addition of 12 μM CHIR99021, the Gsk3 inhibitor. 24 hours after day 0 CHIR addition (day 1), media were changed to regular RPMI with B27 supplement without insulin. On day 3, half of the medium was replaced with fresh RPMI with B27 supplement without insulin, and the addition of 5 μM IWP4, the Wnt signalling inhibitor. On day 5 the media was once again replaced with regular RPMI with B27 supplement without insulin. On day 7, media was replaced with RPMI with B27 supplement with insulin. After this point, the cells were fed every 3 days with RPMI with B27 supplement with insulin. The cells usually began beating between days 8-12.

Metabolic selection

To improve the purity of hiPSC-CMs post differentiation, cells underwent a metabolic selection process after beating was witnessed. This process follows the procedure outlined by Sharma et al.[92] which relies on the ability of hiPSC-CMs to metabolize lactate without depending on glucose as an energy source. In short, the cells were starved of glucose by switching to RPMI without glucose with the addition of B27 supplement with insulin for a period of 3 days. This environment causes cell death of non hiPSC-CMs (e.g., fibroblasts and non-differentiated hiPSCs) because of their inability to use lactate as a fuel source. Afterwards the cells were returned to regular maintenance media. This process is stressful on the cells and tends to lead to a large amount of cell death depending on the quality of the cells, but every surviving cell typically was a beating CM.

Replating

hiPSC-CMs require replating onto round 25 mm #1.5 coverslips for usage in imaging. The coverslips used were a custom made Ibidi polymer coverslip that has better properties for cell attachment and survival than traditional glass coverslips. Prior to replating, coverslips were coated with a 200 µL droplet of matrix for an hour. CMs were then detached with incubation in TrypLE for 5-15 minutes (dependant on cell age), spun down for 4 minutes at 290 RCF, and then resuspended in RPMI with B27 supplement with insulin and ROCK inhibitor. The matrix droplet was then aspirated and replaced with an equal volume of cells, seeding between 50,000-100,000 cells per coverslip, or up to 2,000,000 cells if a monolayer is required. Coverslips with the 200 µL droplet of cells were then incubated overnight at 37 °C for attachment, and then fed with 2 mL of RPMI with B27 supplement with insulin the next day.

SR Ca^{2+} Reporter Construct

pCMV R-CEPIA1er was a gift from Masamitsu Iino (Addgene plasmid #58216)[93] and was used as a base for developing R-CEPIA1$_{SR}$. R-CEPIA1er targets the ER using ER retention signals (i.e., KDEL), therefore the localization signals to the ER were exchanged to transport R-CEPIA1$_{SR}$ to the SR instead via attachment of the SR protein triadin isoform 2 (TRDN) to the 5' end. Triadin cDNA used for the cloning was obtained

through reverse transcription from mRNA. Upon expression, TRDN localizes into the SR, bringing the rest of the reporter construct with it. CEPIAs are based on the GCaMP designs of fluorescent Ca^{2+} indicator proteins, and as such they contain a cp fluorescent protein flanked by a calmodulin (CaM) Ca^{2+} sensing domain and a myosin light chain kinase (M13) domain for binding the calmodulin[94]. This group of indicators was originally designed with cytosolic measurements in mind; however due to the much higher concentrations of Ca^{2+} that CaM is expected to see in the ER/SR, the CaM in R-CEPIA1er has a number of mutations (i.e., E31D/M36L/F92W/E104D/D133E from the calmodulin encoded in GCaMP2 construct) applied to lower its Ca^{2+} affinity, as reflected by an increase in its K_d to 565 μM so that it is able to function without getting saturated under normal conditions[93]. In addition, the fluorescent protein is a cpmApple for a red spectrum fluorescence, freeing up the more commonly used green spectrum for other indicators[95]. While mApple is brighter than other early red fluorescent proteins, it has the unfortunate property of photoswitching when activated[63]. Photoswitching occurs when a fluorophore that has the ability to enter a third state (first and second being rest and excited) is excited for a long period of time (e.g., in the order of seconds). This third state is not excitable at wavelengths normally used to excite the fluorophore resulting in a temporary drop in fluorescence. Fortunately, this state is short-lived and mApple will revert to its rest state after about a minute in the absence of excitation (Figure 6).

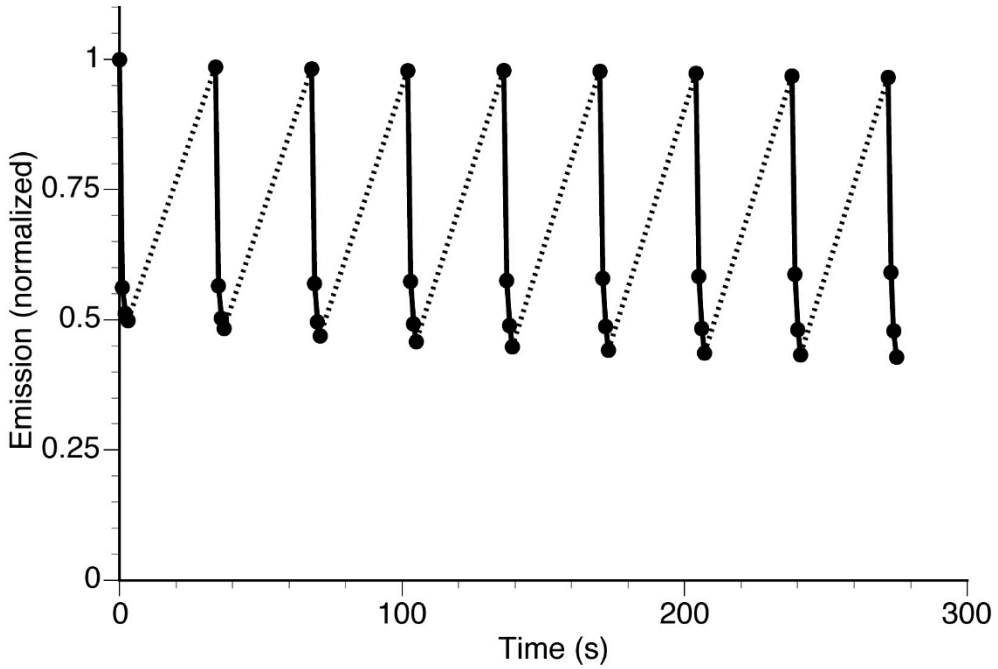

Figure 6: Graph of fluorescence vs time of mApple 0.5 (precursor to mApple) illustrating the photoswitching property.
Solid lines indicate exposure to light activating mApple while dashed lines indicate darkness (no light) conditions. mApple shows a fast drop when excited that quickly recovers in the absence of light. mApple0.5 compared to the final mApple FP lacks the mutations R17H, K92R, S147E, T175A, and T202V, but the final mApple FP still retains this property. Adapted from Shaner et al. 2008[63].

In order to bypass this decrease in fluorescence, the fluorescent reporter cpmApple can be replaced with an alternative cp fluorescent protein for the GCaMP series that is more stable. Unfortunately, there is a lack of any other red cp fluorescent protein, therefore the replacement was reverted to cpEGFP. pCMV G-CEPIA1er was a gift from Masamitsu Iino (Addgene plasmid #58215)[93] and was used as a base for developing G-CEPIA1$_{SR}$ from R-CEPIA1$_{SR}$. The cpEGFP and M13 binding domains were excised from the Addgene G-CEPIA1er and used to replace the equivalent domains on R-CEPIA1$_{SR}$, resulting in a SR Ca^{2+} reporter without problems of photocycling but of the green wavelengths.

Optogenetic Construct

BLINK2 is a light activated K^+ channel based on BLINK1, but with enhanced surface expression that was developed by Anna Moroni in Milan[75]. The construct consists of a small K^+ channel from chlorovirus (Kcv)[96] fused to a LOV2-Jα blue light

sensitive domain that uses Flavin mononucleotide (FMN) as a chromophore from *Avena sativa*[77,97]. In addition, localization signals are included to promote surface expression, including N-terminal myristoylation and palmitoylation sites[98,99], and a C-terminal KAT1 protein fragment for binding 14-3-3 proteins to improve channel activity[75,100]. As BLINK2 does not fluoresce on its own (the LOV2 domain only absorbs light and does not fluoresce), it is conjugated to EGFP via an IRES2 sequence as an indicator for successful expression (Figure 7).

p-mCherry-C1-Phobos was a gift from Peter Hegemann (Addgene plasmid # 98166)[79] and is a light activated Cl^- channel based on the channelrhodopsin C1C2. T159G/G163A mutations were made to a refined version of C1C2 (iC++) in order to blueshift the activation spectrum from 488 nm to 467 nm. Like BLINK2, the construct does not fluoresce on its own, so it is conjugated to mCherry as an indicator of expression and localization.

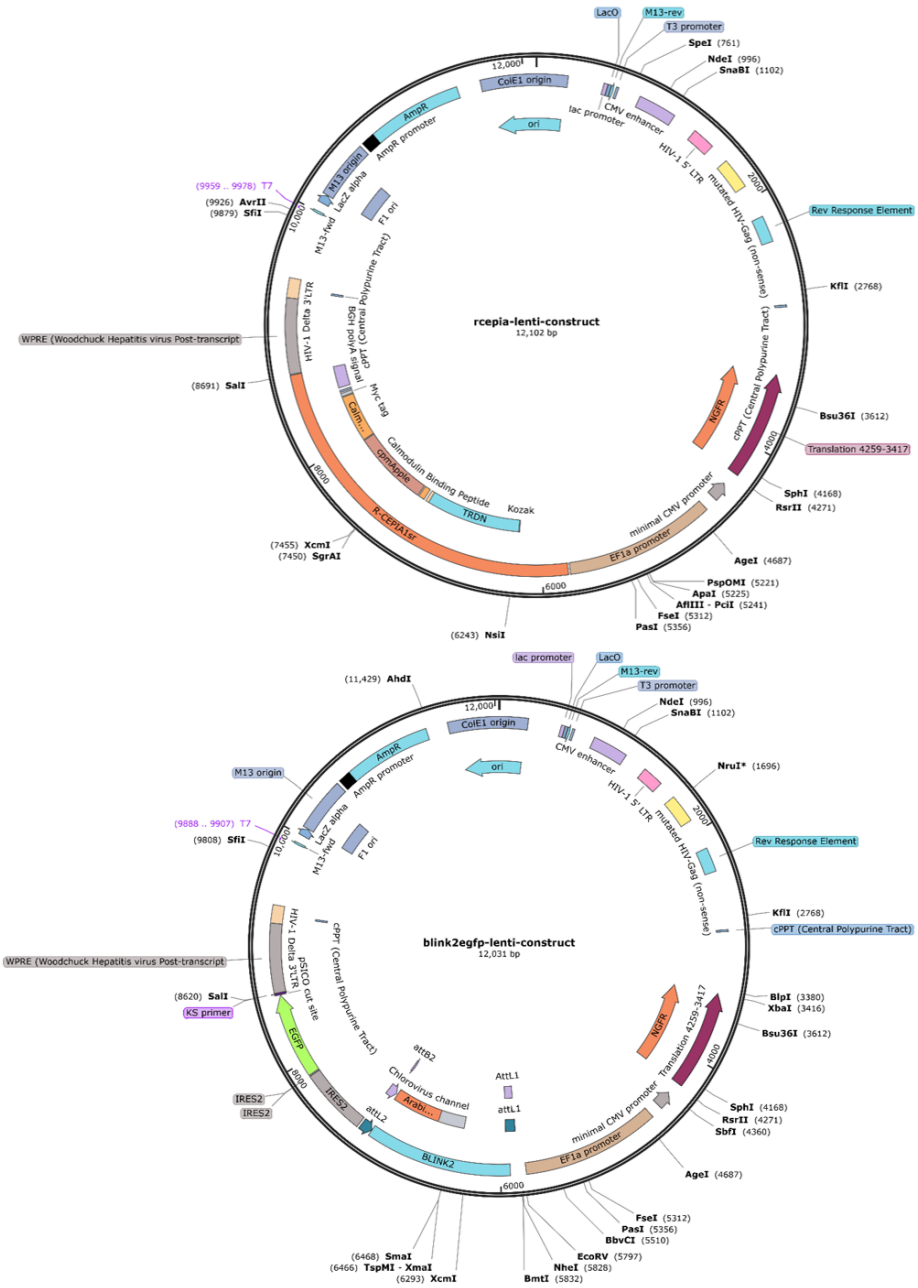

Figure 7: Map of lentiviral vectors for R-CEPIA1$_{SR}$ and BLINK2.
The R-CEPIA1$_{SR}$ construct (top) contains genes encoding TRDN, cpmApple, calmodulin, and a calmodulin binding peptide, followed by WPRE to improve expression levels driven by EF1α promoter. BLINK2 construct (bottom) contains light sensitive domain and chlorovirus channel domain, with an intraribosomal entry site followed by EGFP as a fluorescent indicator of expression. WPRE and promoter sites are the same as the other.

Lentiviral Cloning and Production

3rd generation lentiviral plasmids were a gift from the Megan Levings lab at BCCHR. Plasmids were maintained and expanded in DH5α *E. coli*. Cloning our genes of interest (BLINK2 and R-CEPIA1$_{SR}$) into the lentivirus transfer plasmid used PCR amplification of the genes with compatible restriction enzyme adapters for the plasmid added. Due to the length of the genes (i.e., 1.5 kb and 3 kb, respectively) a high-fidelity polymerase (Phusion) was used to minimize the chance of errors occurring. After restriction digest and cloning, the completed plasmids were fully sequenced across the insertion area to ensure no errors arose at any point (Figure 7). Initial lentiviral vector designs did not include a WPRE site, however one was included after low protein expression levels were found after the construct was successfully introduced into cells.

Lentiviral production utilized HEK293T cells for assembling the completed virus. HEK293T cells used DMEM with 10% FBS as its maintenance media and were passaged once every 3-4 days upon reaching ~70% confluency at a ratio of 1:20. Cells were transfected using lipofectamine 3000 in Opti-Mem with the lentiviral transfer plasmid and all 3 helper plasmids in a single transfection at a ratio of 4:2:1:1 for the transfer, pkg, envelope, and rev plasmids respectively. Cells were incubated for 6 hours and then had their media replaced with regular DMEM with 10% FBS supplement. 48 hours post-transfection, the supernatant was harvested, ultra-centrifuged for concentration, and then stored at -80 °C.

Lentiviral titer (copies/volume) was determined using a commercially available qPCR based lentiviral titer kit from ABMGood (ABMGood catalogue #: LV-900). Reactions were made according to the manufacturer's instructions in a 96 well plate in triplicate and run on a Bio-Rad thermocycler.

Transduction

The number of hiPSC-CMs must be known prior to transduction (infection) with the lentivirus. As hiPSC-CMs are post-mitotic and non-dividing, the initial number seeded onto the coverslips is assumed to be the final cell count. An appropriate amount of virus was added to the media of the coverslips, based on the titer, to reach expected multiplicity of infections (MOIs; number of viable viral particles per cell). Cells were

incubated for 5 days, with the media being changed as necessary to ensure the removal of all remaining viable lentivirus before being used for downstream applications. For our hiPSC-CMs we found an MOI of 6 to be the optimal balance between expression level and toxicity. Expression was confirmed via presence of fluorescent signals (EGFP for BLINK2 or mApple for R-CEPIA1$_{SR}$).

CRISPR Construct

BLINK2 and R-CEPIA1$_{SR}$ were linked via T2A self-cleaving peptide and expressed under a single promoter as a bicistronic protein (Figure 8). Due to localization signal requirements on the 5' end of BLINK2, it was placed first with R-CEPIA1$_{SR}$ following it. The construct was then integrated into the CLYBL genomic safe harbour site of hiPSCs with the assistance of the BCCHR core facility headed by Francis Lynn using the CRISPR/Cas9 system. hiPSCs were then selected via puromycin and screened for red fluorescence indicative of R-CEPIA1$_{SR}$ expression and those shown to be expressing were then isolated and expanded into monoclonal colonies. Afterwards, proper integration into the CLYBL site was determined via PCR amplification across the arms of the insertion site (Figure 9). Those showing proper integration were differentiated into hiPSC-CMs and imaged to determine proper function.

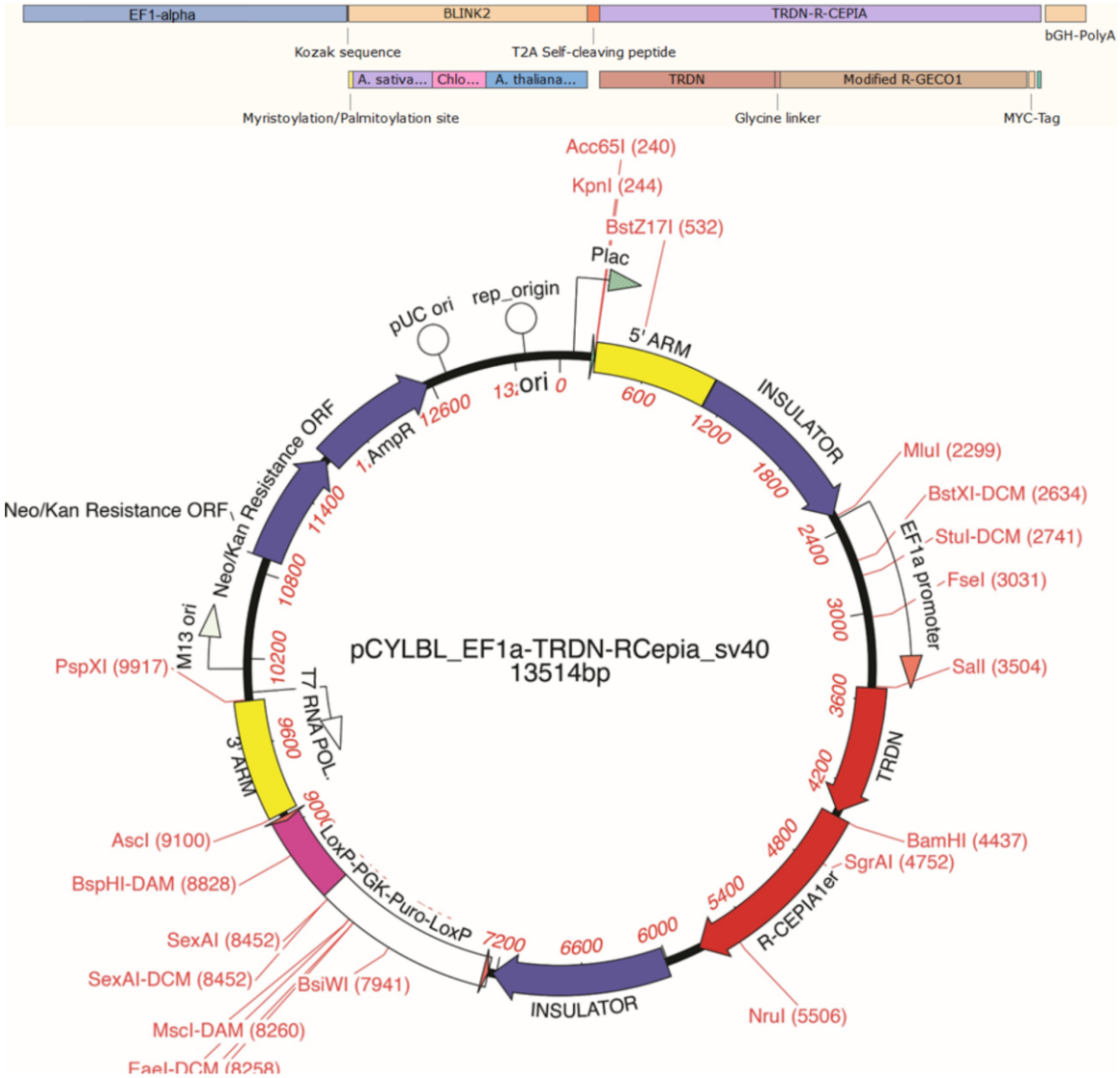

Figure 8: BLINK2/R-CEPIA1$_{SR}$ bicistronic CRISPR construct
Top: BLINK2/R-CEPIA1$_{SR}$ CRISPR construct, connected together via self-cleaving peptide. On expression in the cell, BLINK2 and R-CEPIA1$_{SR}$ will separate into two different proteins to localize to their required locations. Bottom: Final construct for R-CEPIA1$_{SR}$ used in CRISPR/Cas9 insertion into CLYBL genomic safe harbour site. From Arslanova et al. 2022[101]

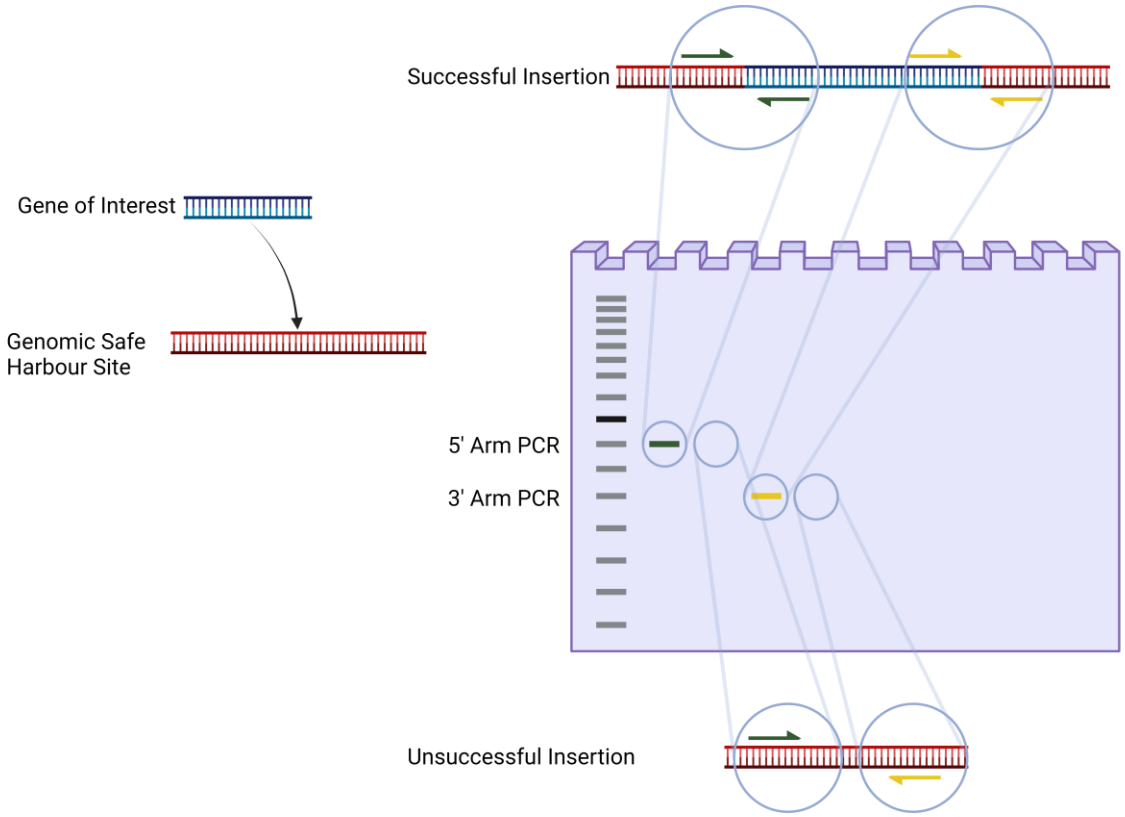

Figure 9: PCR verification of successful CRISPR insertion
PCR amplification used to determine successful insertion of a gene (blue) into a safe harbour site (red) via CRISPR/Cas9. PCR amplification across arms of insertion site is expected to only produce bands on successful integration. Without integration, arms covering the blue gene would not bind and therefore no amplification would occur.

Imaging/Calibration of R-CEPIA1$_{SR}$

Fluorescent indicators for cytosolic Ca^{2+} for R-CEPIA1$_{SR}$ imaging utilized Calbryte-520 AM dye from AAT Bioquest (catalogue #: 20650) and Calbryte-630 AM (catalogue #: 20720) for BLINK2. An hour prior to imaging, cells were loaded with 1-5 µM of the relevant dye at 37 °C depending on the preferred fluorescence level. Coverslips were placed in a fluidic chamber (i.e., Chamlide made by Live Cell Instrument) for imaging. The chamber was open to the environment to allow for application of drugs and other direct manipulations and comes with inflow and outflow lines for exchanging media, as well as a set of electrodes for field stimulation. Due to the cytotoxicity of the dyes and the non-sterile imaging environment, all experiments were terminal.

All imaging was performed on a Leica SP8 confocal microscope. This microscope is equipped with a white light laser (WLL) capable of illuminating up to 8 different wavelengths between 470-670 nm, at 1.5 mW/nm power, by utilizing an acousto-optical beam splitter (AOBS) instead of dichroic mirrors. The WLL was run at 70% power as recommended by the facility manager of the instrument, Jingsong Wang. Imaging was done at 63x magnification using glycerine immersion lens to image single cells. Through the use of a resonant scanner for scanning at 8000 Hz, a frame rate of ~30 frames per second was achieved. The SP8 automatically translates detected field fluorescence to a quantity, which was used to determine relative Ca^{2+} levels.

As R-CEPIA1$_{SR}$ emits a red fluorescent signal, it was paired with a green cytosolic Ca^{2+} dye Calbryte-520. For BLINK2, it carries an EGFP as a fluorescent indicator to indicate expression, so it was paired with a red cytosolic Ca^{2+} dye, Calbryte-630. Calbryte-520 was excited at 488 nm and detected at 500-540 nm, R-CEPIA1$_{SR}$ was excited at 570 nm and detected at 580-700 nm, Calbryte-630 was excited at 605 nm and detected at 615-700 nm, and BLINK2 was excited at 470 nm.

As imaging of R-CEPIA1$_{SR}$ requires the use of two fluorophores (R-CEPIA1$_{SR}$ and one for cytosolic Ca^{2+}), spectral overlap was a challenge. The crosstalk of one brightly fluorescing reporter can overwhelm the signal of the other and completely mask it. To help address this, the Acousto-Optical Beam Splitters (AOBS) on the Leica SP8 are capable of tuning the transmittance separately for each individual wavelength transmitted through it. Using this property, the amount of power used for exciting the brighter reporter (Calbryte-520) was lowered while the power for the dimmer reporter (R-CEPIA1$_{SR}$) was increased. In addition, the amount of Calbryte-520 loaded was also reduced (1 μM instead of 5 μM) to further lower its fluorescence signal. Through these methods both signals could be brought to relatively equal levels, allowing a noticeable change in fluorescence in both reporters in response to changes in Ca^{2+}. Temporal gating was utilized to reduce auto-fluorescence from the coverslip and from dead cells. I used 1-6 ns gating for R-CEPIA1$_{SR}$ and 0.3-6 ns gating for Calbryte520.

Cells were imaged using Tyrode's solution (Table 2) as the media and paced using an external stimulation box (Harvard Apparatus) at 1 Hz for all recordings. The media that the cells were exposed to was exchanged using a peristaltic pump at a constant flow rate in order to wash out any drugs to which the cells were exposed. To

limit movement artifacts due to the beating of the hiPSC-CMs, the cells were exposed to 5 μM of mavacamten to inhibit myosin ATPase to uncouple the contraction machinery from the Ca^{2+} handling. For the application of drugs that require an instantaneous response such as caffeine, I utilized a MicroFil needle positioned next to the field of view allowing for immediate direct delivery into the field of view; otherwise, drugs were applied by exchanging the bath media manually.

Table 2: Tyrode's Solution formula

Compound	Concentration (mM)
NaCl	117
KCl	5.7
$NaHCO_3$	4.4
NaH_2PO_4-H_2O	1.5
$MgCl_2$	1.7
Na-HEPES	10
Creatine	5
Na-Pyruvic Acid	5
$CaCl_2$	1.8
Glucose	5

Image Processing

Due to the low brightness of signals from R-CEPIA1$_{SR}$, fluorescence data had a very low signal to noise ratio. To better visualize fluorescence readings, data underwent filtering through a Bessel filter program written in Matlab by Shayan Jannati, with a cut-off frequency of 2.5 Hz in order to reduce noise (Figure 10). Higher frequencies showed less effective reduction in noise, while lower frequencies lowered amplitude and made it difficult to see smaller signals. Due to also having a separate cytosolic Ca^{2+} indicator simultaneously, R-CEPIA1$_{SR}$ signal could be compared in order to determine the exact location of every expected peak, a 2.5 Hz cut-off frequency was therefore determined to have the best balance between reducing noise while retaining noticeable signal.

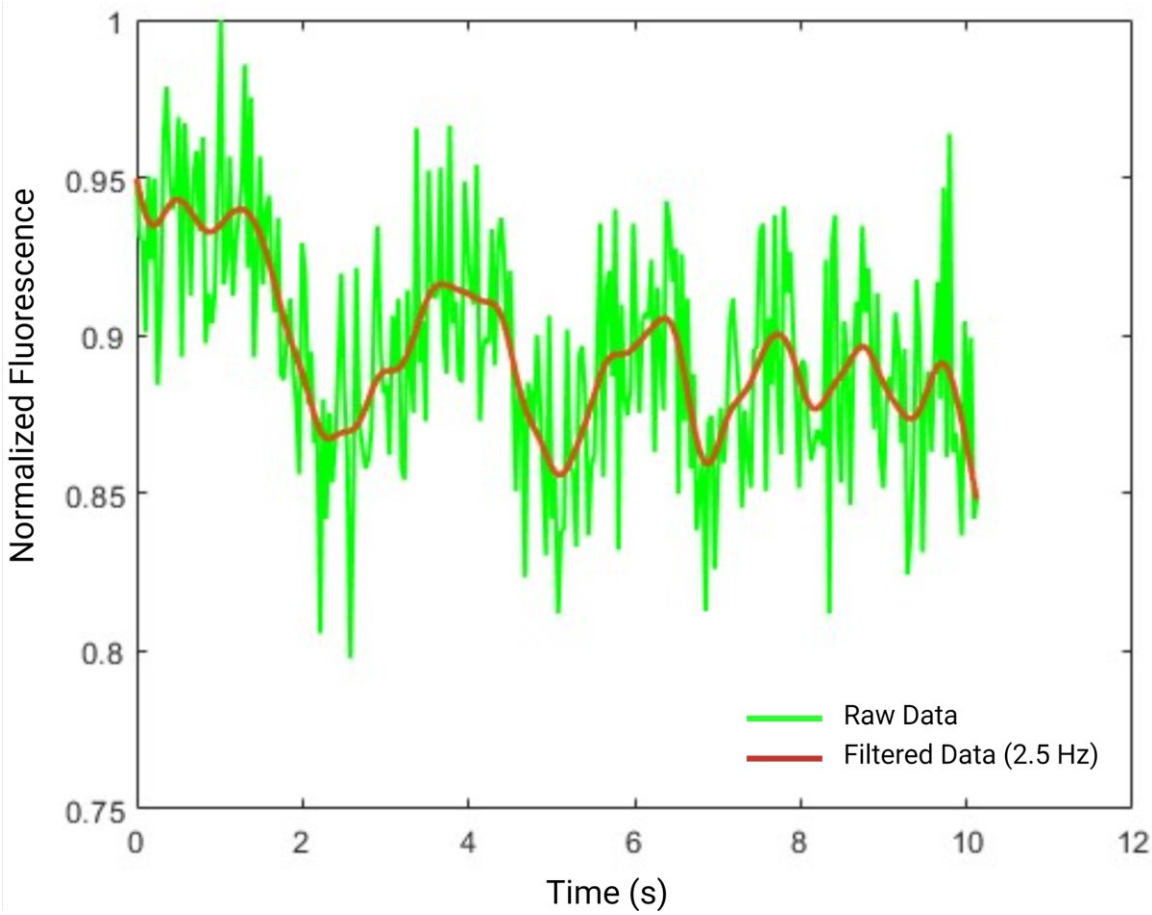

Figure 10: Matlab Bessel filter reducing noise from fluorescence graph at 2.5 Hz.

Green line represents the raw data while the red line represents the new filtered data. The large amount of noise makes the small changes in fluorescence from R-CEPIA1$_{SR}$ difficult to see before filtering but become much clearer afterwards.

Results

CRISPR/Cas9 integration into the genomic safe harbour site CLYBL

Cloning of plasmids containing BLINK2 was unsuccessful; bacteria transformed with BLINK2 and plated onto selection media showed no positive clones. This could be due to problems in the cloning process resulting in the plasmid failing to circularize, or adverse reactions of the bacteria to BLINK2 due to its viral origins. Due to issues in the cloning of BLINK2, only R-CEPIA1$_{SR}$ was used for the integration. PCR amplification across the integration arms showed expected bands although some samples were very faint (Figure 11). 10 clones in total (4 homozygous, 6 heterozygous) were selected and cryopreserved.

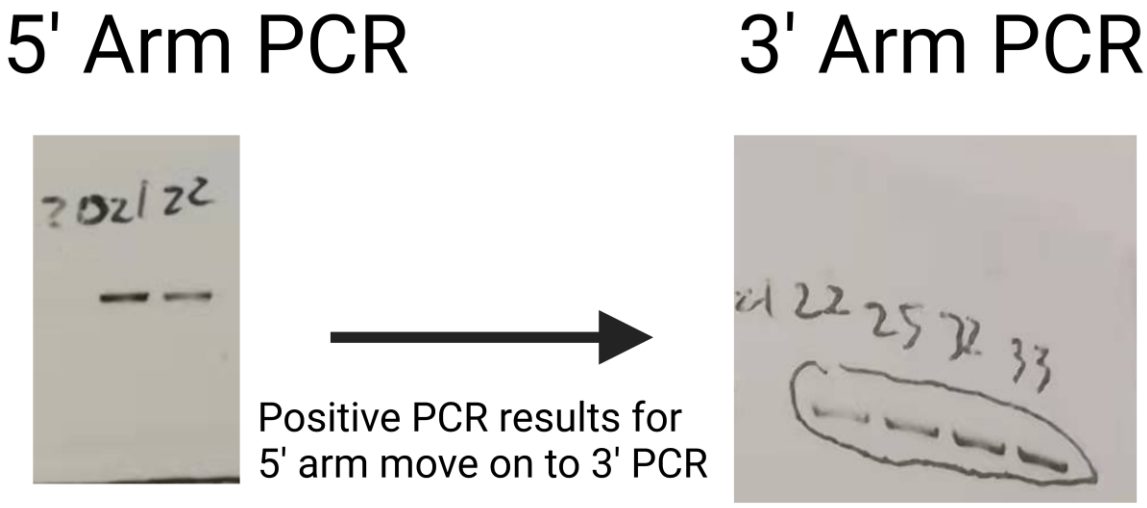

Figure 11: PCR bands across the integration site of CLYBL checking for proper integration of R-CEPIA1$_{SR}$
This figure illustrates the PCR amplification across integration sites starting with the 5' arm to show successful integration. Clones that show successful integration move on to the 3' arm to confirm the other side. Clones that show a visible band of the right sizes are considered to have properly integrated via CRISPR/Cas9.

A heterozygous clone was differentiated into hiPSC-CMs successfully, however red fluorescence from R-CEPIA1$_{SR}$ was not found. A possible reason for this could be that the insertion site was inactivated upon differentiation from hiPSC to hiPSC-CMs, however upon imaging the hiPSCs that the CMs were derived from, it was found that red fluorescence was nearly non-existent. This result suggests that loss of R-CEPIA1$_{SR}$

expression was independent from differentiation and was either lost from the genomic safe harbour site over time or alternatively, due to the “heterozygous” colony not being actually monoclonal and instead were contaminated with unintegrated hiPSCs. These unintegrated hiPSCs could outcompete the R-CEPIA1$_{SR}$ expressing hiPSCs over time and become the dominant cell type.

The differentiation was reattempted with homozygous R-CEPIA1$_{SR}$ expressing hiPSCs to eliminate the possibility of contaminating hiPSCs. Similar to the heterozygous differentiation, hiPSC-CMs were found to lack any notable red fluorescence. hiPSCs were imaged right after thawing, and again after 2 months with the exact same settings. hiPSCs showed a full coverage of red fluorescence when imaged right after thawing while imaging after 2 months showed very few red fluorescent cells remaining (Figure 12). From this result it is likely that the CLYBL site, although allows high expression in hiPSCs, is not stable enough for the long-term integration that is necessary for hiPSC-CMs due to the differentiation processes.

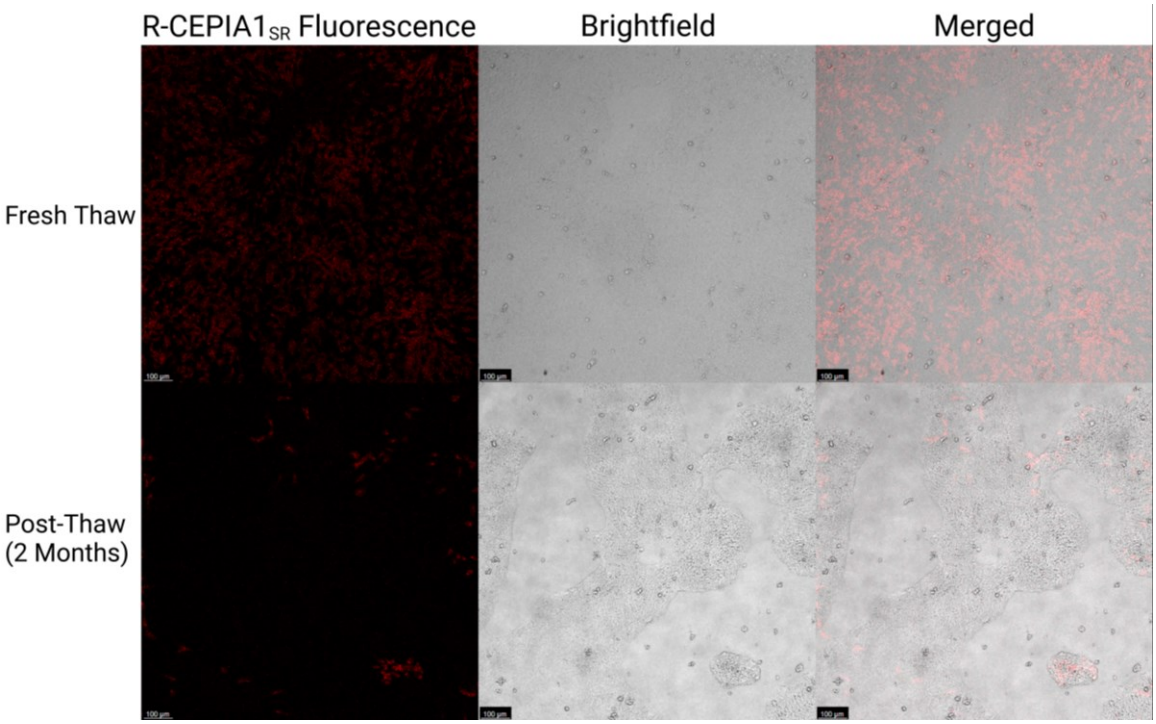

Figure 12: hiPSCs with genome inserted R-CEPIA1$_{SR}$ after thaw and two months later.

hiPSCs with homozygous R-CEPIA1$_{SR}$ inserted into the genomic safe harbour site CLYBL via CRISPR/Cas9 system. Cells were imaged for red fluorescence after thawing and again after two months. hiPSCs showed a notable decrease in red fluorescence after 2 months indicating loss of R-CEPIA1$_{SR}$ over time.

Phobos

Phobos was expressed in hiPSC-CMs via lentiviral transduction. The cells containing the construct using the Lecia SP5 confocal microscope. The SP5's Argon laser was used to activate Phobos at 476 nm, while the Helium Neon 543 nm laser was used to excite the cytosolic Ca^{2+} indicator Calbryte-630 to track beating in the form of Ca^{2+} transients. Unfortunately, activation of Phobos failed to hold the cell at a depolarized membrane potential strong enough to prevent beating (Figure 13). However Phobos was shown to be functional in allowing the passage of ions in response to light.

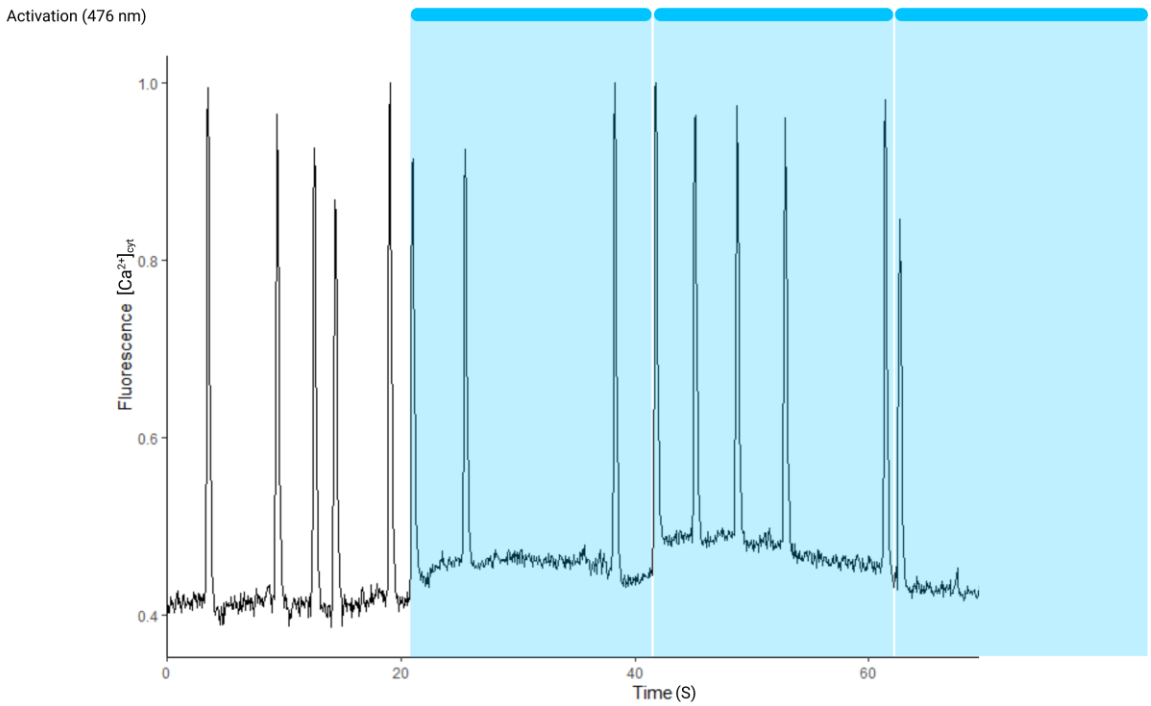

Figure 13: Fluorescence trace of cytosolic Ca^{2+} over time with activation of Phobos in hiPSC-CMs.
Constant activation of the Cl^- channel Phobos does not lead to cessation of spontaneous action potentials.

Since the activation of Phobos which allows the flow of Cl^- out of the cell causes a depolarization in membrane potential, activating voltage gated ion channels, and resulting in a full action potential, Phobos could theoretically also be used to optically pace the cell (as opposed to pacing through electrode stimulation). Indeed, activation of Phobos consistently showed that the cells would immediately go through a contraction

cycle, and by toggling the activation laser on and off the cells could be paced (Figure 14) although continuous activation was not enough to prevent further depolarizations.

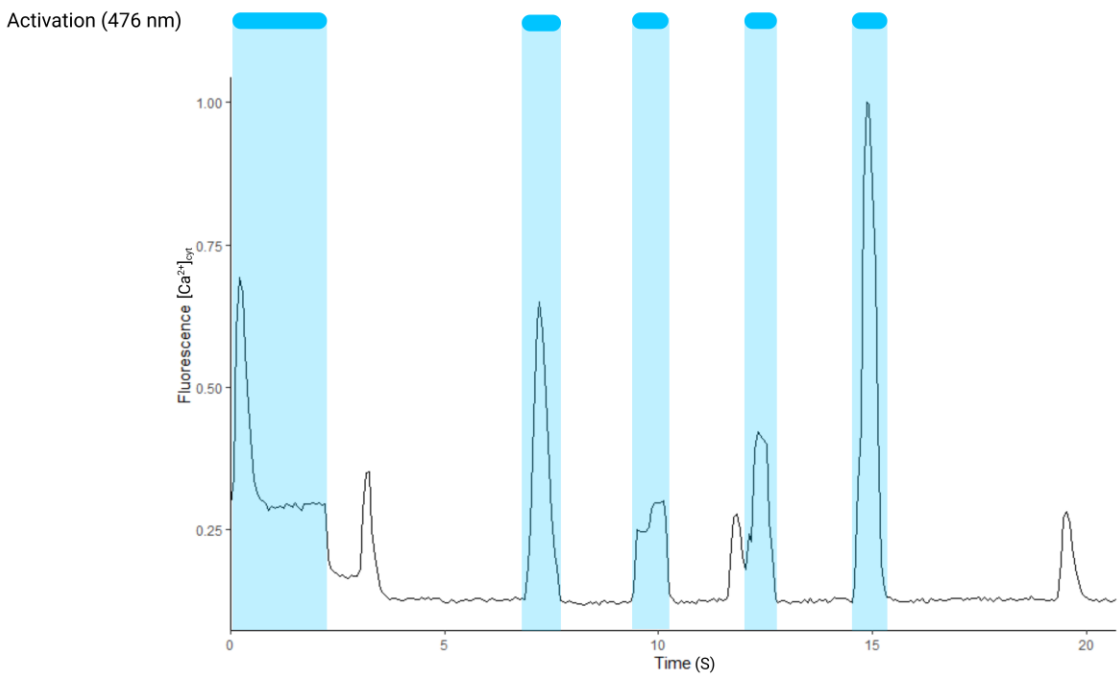

Figure 14: Fluorescence trace of cytosolic Ca^{2+} over time in Phobos expressing cells using activation to depolarize the cells.
Activation of Phobos with 476 nm light allows passage of Cl^- ions resulting in depolarizations and allowing pacing of the CMs.

BLINK2

BLINK2 was expressed in hiPSC-CMs via lentiviral transduction. The Leica SP8 white light laser is capable of excitation at a range of 470 nm to 670 nm, and 405 nm using the UV diode, so the maximum absorbance of BLINK2 through FMN (~450 nm) is outside of its range. FMN's absorption spectrum sharply drops at about ~470 nm, as well as at ~400 nm it is also fairly low making these wavelengths not ideal for activating BLINK2. Attempts at illuminating the hiPSC-CMs with both 470 and 405 nm laser concurrently did not result in cessation of spontaneous beating.

Attempts at using an argon laser which is capable of illuminating at 458 nm also failed to reach quiescence. Part of the reason could be too low of an expression of the channel at the cell surface to cause a large enough K^+ current that will hyperpolarize the cell. Future attempts can be made at a higher lentiviral MOI to increase expression

levels of BLINK2 or performed in a slightly hypokalemic solution to maximize the activity of the channels that do exist.

R-CEPIA1$_{SR}$ calibration

Lentiviral transduction of R-CEPIA1$_{SR}$ at MOI 6 showed the expected red signal from the mApple fluorescent protein in R-CEPIA1$_{SR}$. Lower MOIs were attempted with limited success. Concurrent imaging with Calbryte-520 initially showed only changes in fluorescence due to Calbryte-520 in both channels used to pick up cytosolic (green/Calbryte-520) Ca^{2+} and SR (red/R-CEPIA1$_{SR}$) Ca^{2+} levels. This was due to the high amount of fluorescent signal coming from Calbryte-520 (Figure 15, Figure 16). R-CEPIA1$_{SR}$ excitation laser transmittance was increased from 10% to 50% to help improve the red fluorescent signal, however Calbryte-520's emission was still too high and overwhelming the R-CEPIA1$_{SR}$ signal. By reducing the amount of Calbryte-520 from 5 μM to 1 μM and reducing transmittance of power from 5% to 0.1%, Calbryte-520 fluorescence was lowered to a comparable level to R-CEPIA1$_{SR}$ emission levels. Signals from this imaging showed dips in the R-CEPIA1$_{SR}$ signal at the same time as an increase in the Calbryte-520 signal (Figure 17). This indicates a decrease in $[Ca^{2+}]_{SR}$ at the same time as $[Ca^{2+}]_{Cytosol}$ increased, as would be expected if RyR2 opened to release Ca^{2+} in the SR to the cytosol. Interestingly, pacing the cells at 1 Hz is higher than the intrinsic spontaneous beat rate of the cells, and upon stimulation the R-CEPIA1$_{SR}$ signal's dynamic range decreases (magnitude of change in fluorescence signal in the presence of Ca^{2+}). Cytosolic Ca^{2+} levels stayed the same for systole while diastole levels increased. For SR Ca^{2+} levels, diastole levels stayed the same while systole did not drop as much. This could be because the increased Ca^{2+} cycling rate was faster than Ca^{2+} extrusion mechanisms such as NCX could remove Ca^{2+} (Figure 18).

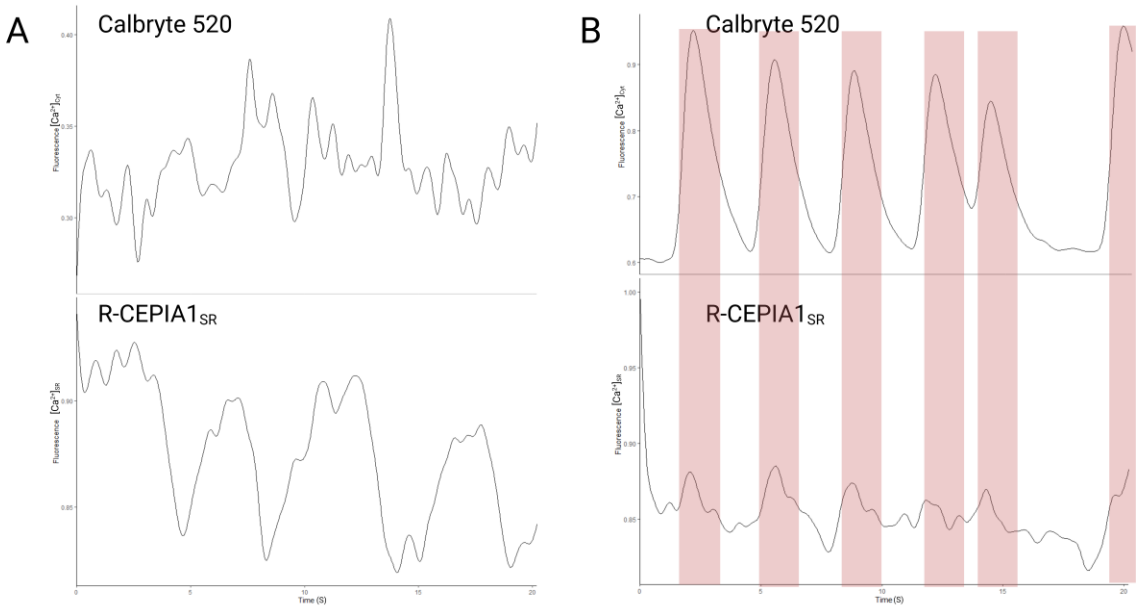

Figure 15: Fluorescence trace graphs of cytosolic and SR Ca^{2+} in R-CEPIA1$_{SR}$ expressing cells with and without 488 nm laser showing obvious crosstalk between channels.

A) Imaging of hiPSC-CMs transduced with R-CEPIA1$_{SR}$ without excitation of Calbryte-520 cytosolic Ca indicator. R-CEPIA1$_{SR}$ shows dips in fluorescence indicating SR Ca^{2+} release. B) Activation of green laser for exciting Calbryte-520 results bleeding into and overwhelming the R-CEPIA1$_{SR}$ signal despite the separation in wavelengths.

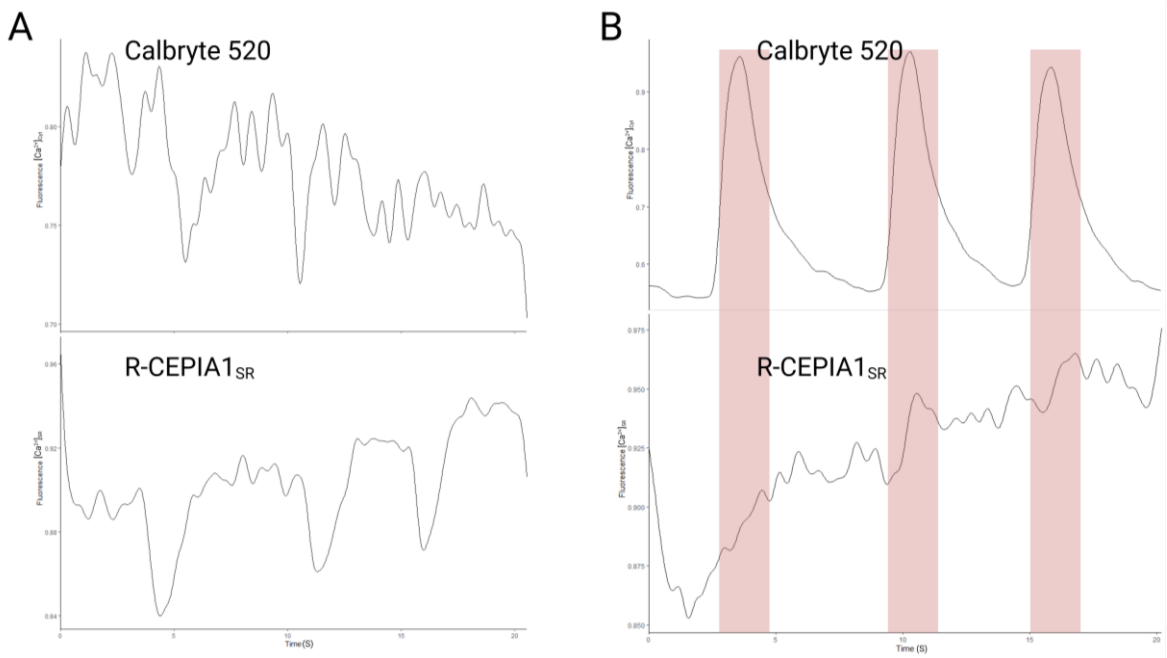

Figure 16: Fluorescence trace graphs of cytosolic and SR Ca^{2+} in R-CEPIA1$_{SR}$ expressing cells with and without 488 nm laser showing crosstalk masking R-CEPIA1$_{SR}$ signal.

A) Imaging of hiPSC-CMs transduced with R-CEPIA1$_{SR}$. Green Calbryte-520 excitation laser is turned off and R-CEPIA1$_{SR}$ signal show clear dips as SR Ca^{2+} is released. B) Activation of Calbryte-520 excitation laser results in bleed through to the R-CEPIA1$_{SR}$ channel. Although not immediately apparent on its own, when taking into account the R-CEPIA1$_{SR}$ signal without Calbryte-520 excitation, the spectral overlap results in masking of the R-CEPIA1$_{SR}$ signal from Calbryte-520 making it indistinguishable from baseline noise.

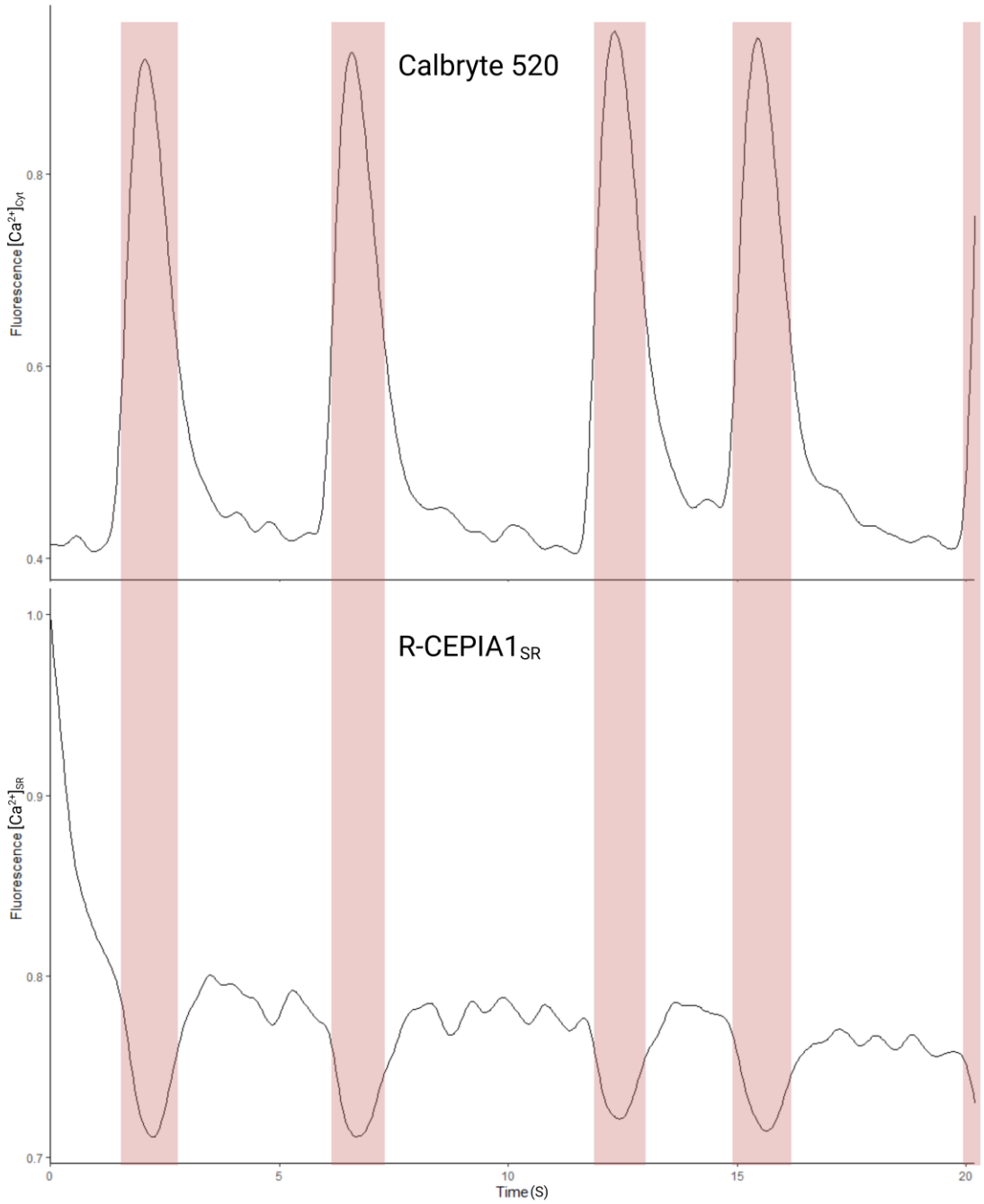

Figure 17: Fluorescence trace graphs of cytosolic and SR Ca^{2+} in R-CEPIA1$_{SR}$ expressing cells reporting Ca^{2+} in both.

R-CEPIA1$_{SR}$ reacting to and reporting changes in SR Ca^{2+} levels. Top: Calbryte-520 fluorescence signal, increase in Y indicates increase in cytosolic Ca^{2+} levels. Bottom: Red signal from R-CEPIA1$_{SR}$, decreases in Y indicate drops in SR Ca^{2+} levels. Both signals imaged concurrently and are plotted on the same X axis (time). Red boxes highlighting peaks of cytosolic Ca^{2+} transients correspond closely with the nadir of the R-CEPIA1$_{SR}$ signal.

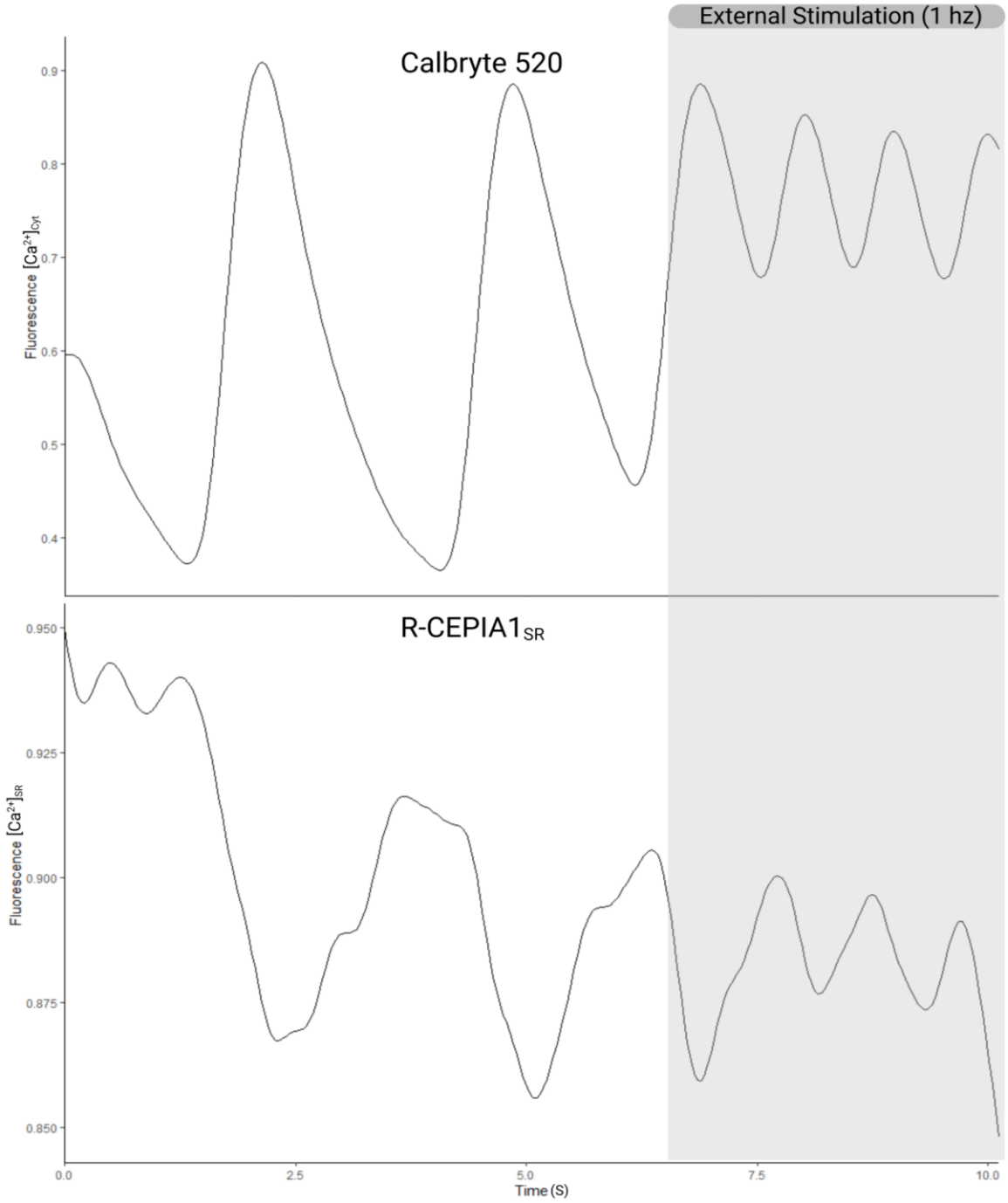

Figure 18: Fluorescence trace graphs of cytosolic and SR Ca^{2+} in R-CEPIA1$_{SR}$ expressing cells with external stimulation pacing cells.

Spontaneous and paced R-CEPIA1$_{SR}$ signals. Pacing at 1 Hz was faster than spontaneous beat rate, resulting in a lower dynamic range of signal in both Calbryte-520 (cytosolic) and R-CEPIA1$_{SR}$ (SR) Ca^{2+} levels.

The R-CEPIA1$_{SR}$ signal was found to be unstable; the signal tended to drop quickly over a short period of time (<1 min), resulting in a decrease in the dynamic range, and eventually reaching a point in which the signal was nearly indistinguishable from noise (Figure 19) This could be due to mApple photobleaching or possibly from mApple's photoswitching properties. To avoid this, recordings were kept as short as possible.

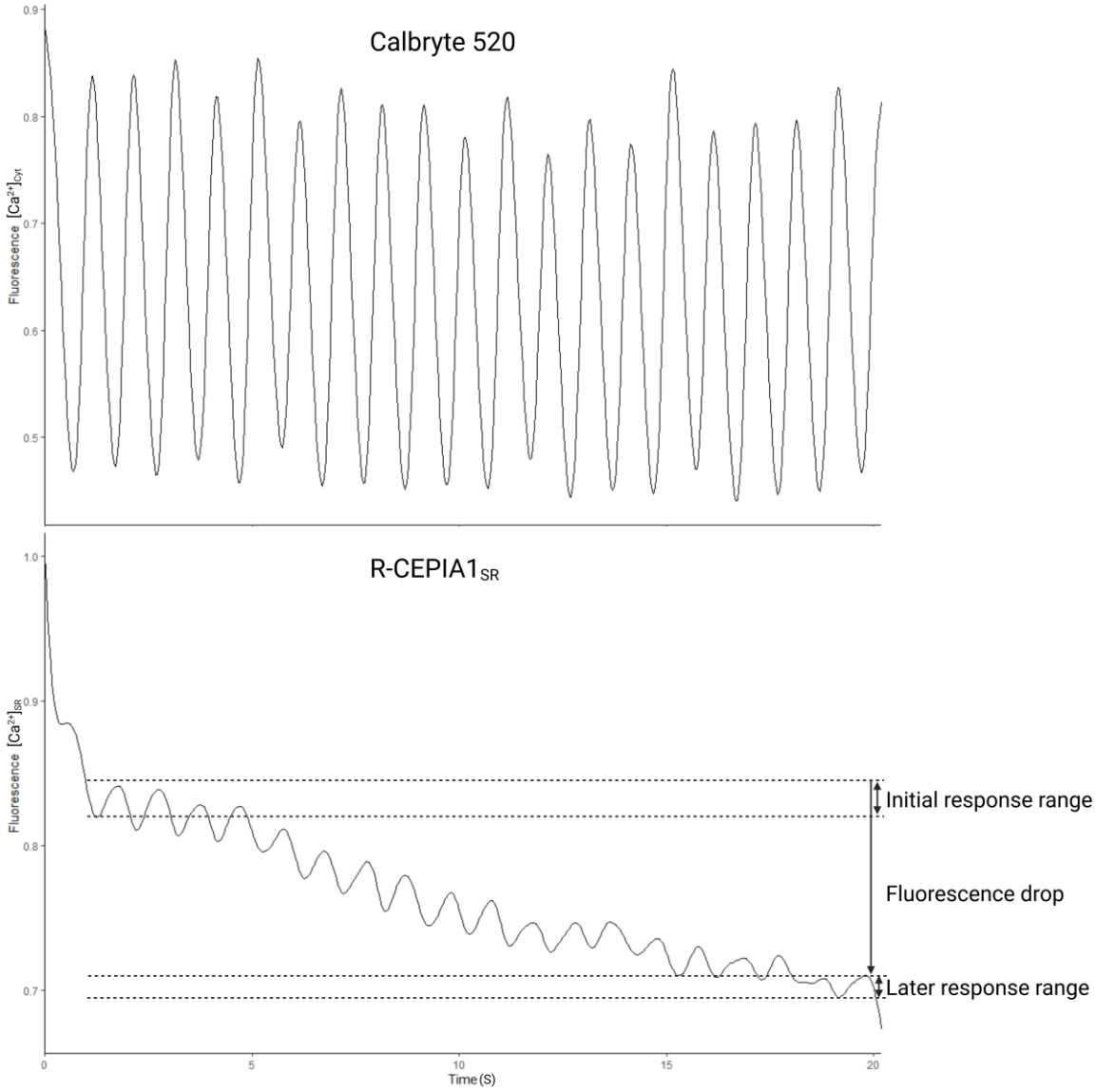

Figure 19: Fluorescence trace graphs of cytosolic and SR Ca^{2+} in R-CEPIA1$_{SR}$ expressing cells over longer recordings showing gradual decrease in fluorescence.

R-CEPIA1$_{SR}$ signal range gradually decreasing over a 20 second recording. Decrease possibly due to photobleaching or more likely photoswitching properties of the R-CEPIA1$_{SR}$ fluorophore mApple.

Application of caffeine to fully open all RyR2 and empty the SR of Ca^{2+} showed the expected response in R-CEPIA1$_{SR}$ signal. Post-caffeine exposure loading of the SR requires the washout of all remaining caffeine, as well as stimulation to allow for the opening of L-type calcium channels to increase $[Ca^{2+}]_{Cytosol}$ and allow SR loading, before R-CEPIA1$_{SR}$'s signal slowly recovers (Figure 20). The R-CEPIA1$_{SR}$ signal increased slightly in fluorescence during recovery but did not retain the same dynamic range as at the start of the recording, either because the SR had not recovered to the same level, or because of a decrease in R-CEPIA1$_{SR}$ brightness and therefore responsiveness over time during imaging, or a combination of both. Longer recordings were also difficult due to the aforementioned decrease in fluorescence of R-CEPIA1$_{SR}$ over time.

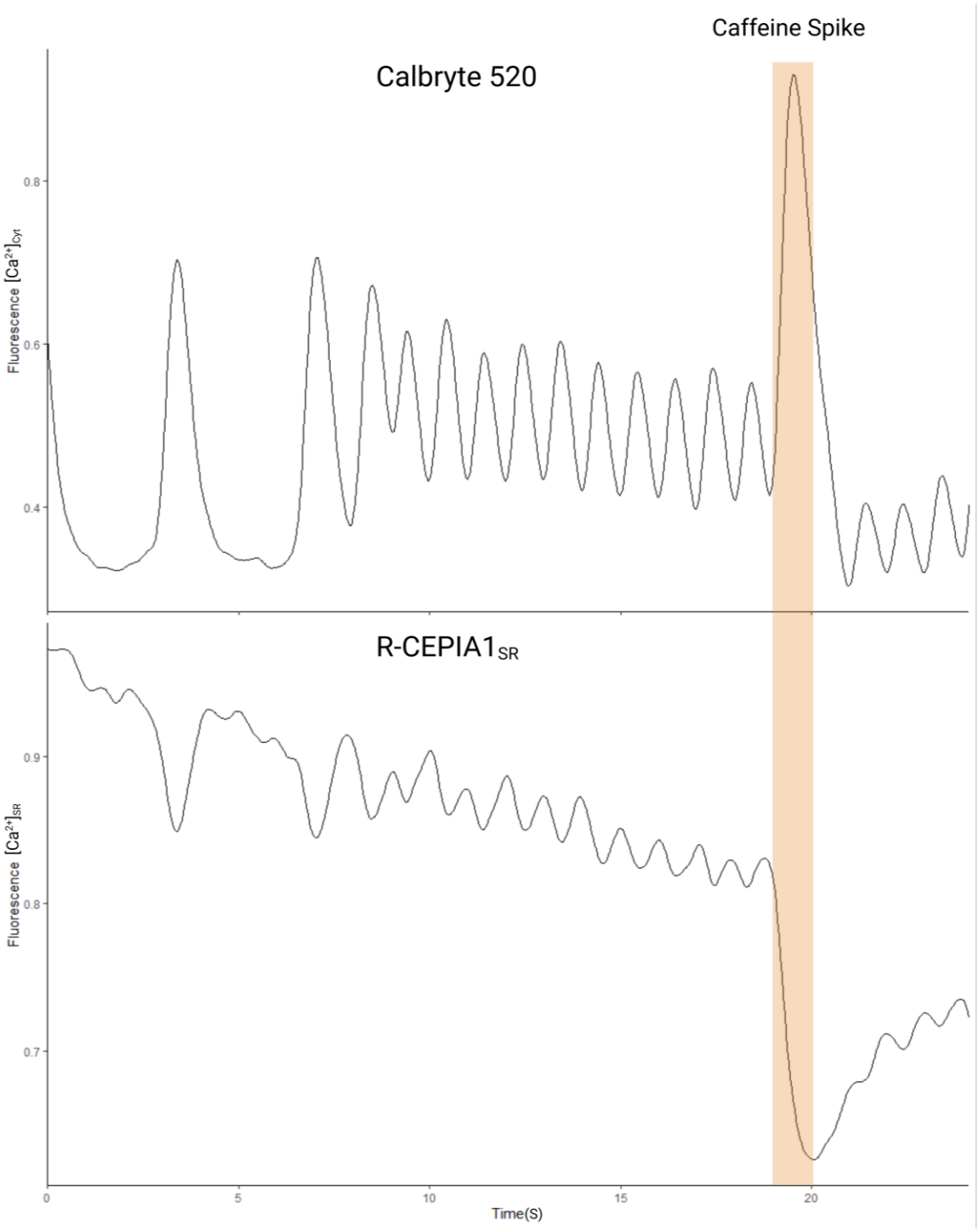

Figure 20: Fluorescence trace graphs of cytosolic and SR Ca^{2+} in R-CEPIA1$_{SR}$ expressing cells with exposure to caffeine.

R-CEPIA1$_{SR}$ shows a large drop in $[Ca^{2+}]_{SR}$ upon exposure to caffeine (orange). Addition of caffeine is expected to fully open RyR2 and empty SR of Ca^{2+}. SR slowly loads again afterwards indicated by gradual increase in R-CEPIA1$_{SR}$ fluorescence

To improve the signal during longer recordings in order to measure the full recovery of SR Ca^{2+} levels after depletion, methods to circumvent the decrease in fluorescence of R-CEPIA1$_{SR}$ and maintain its responsiveness are required. Photobleaching is an irreversible process that occurs with stronger laser illumination, however R-CEPIA1$_{SR}$ signal is already very low with the current settings, so lowering it further is not a viable solution unless paired with methods to increase the signal independently, such as increasing expression levels of R-CEPIA1$_{SR}$ through either modifications to the construct, or simply increasing gene dosage (number of copies of a gene) via higher MOI transductions, at the risk of increased lentiviral toxicity. An alternative problem that can be more easily addressed is the photoswitching.

Photoswitching is a property known for mApple that results in the production of a third state other than its ground and excited states. This third state is unresponsive to the same wavelengths of light as the ground and does not emit the same wavelength of light as the excited state but is unstable and will quickly revert back to the ground state. Based on this, a longer R-CEPIA1$_{SR}$ imaging was attempted with the inclusion of a rest period (without R-CEPIA1$_{SR}$ excitation) to allow all non-photobleached R-CEPIA1$_{SR}$ to revert back to ground state. As the SP8 excitation wavelengths can be individually adjusted this can be done without impacting other fluorescent reporters such as Calbryte-520. R-CEPIA1$_{SR}$ was able to successfully maintain responsiveness, even for a full minute after recording started, if a 30 second rest period (Figure 21) was introduced. Through this method the important temporal periods, such as during drug additions, can be recorded specifically. This comes at the cost of having some temporal gaps in the recording data however and can still be an issue if the critical recording times are required to be uninterrupted and longer than 30 seconds.

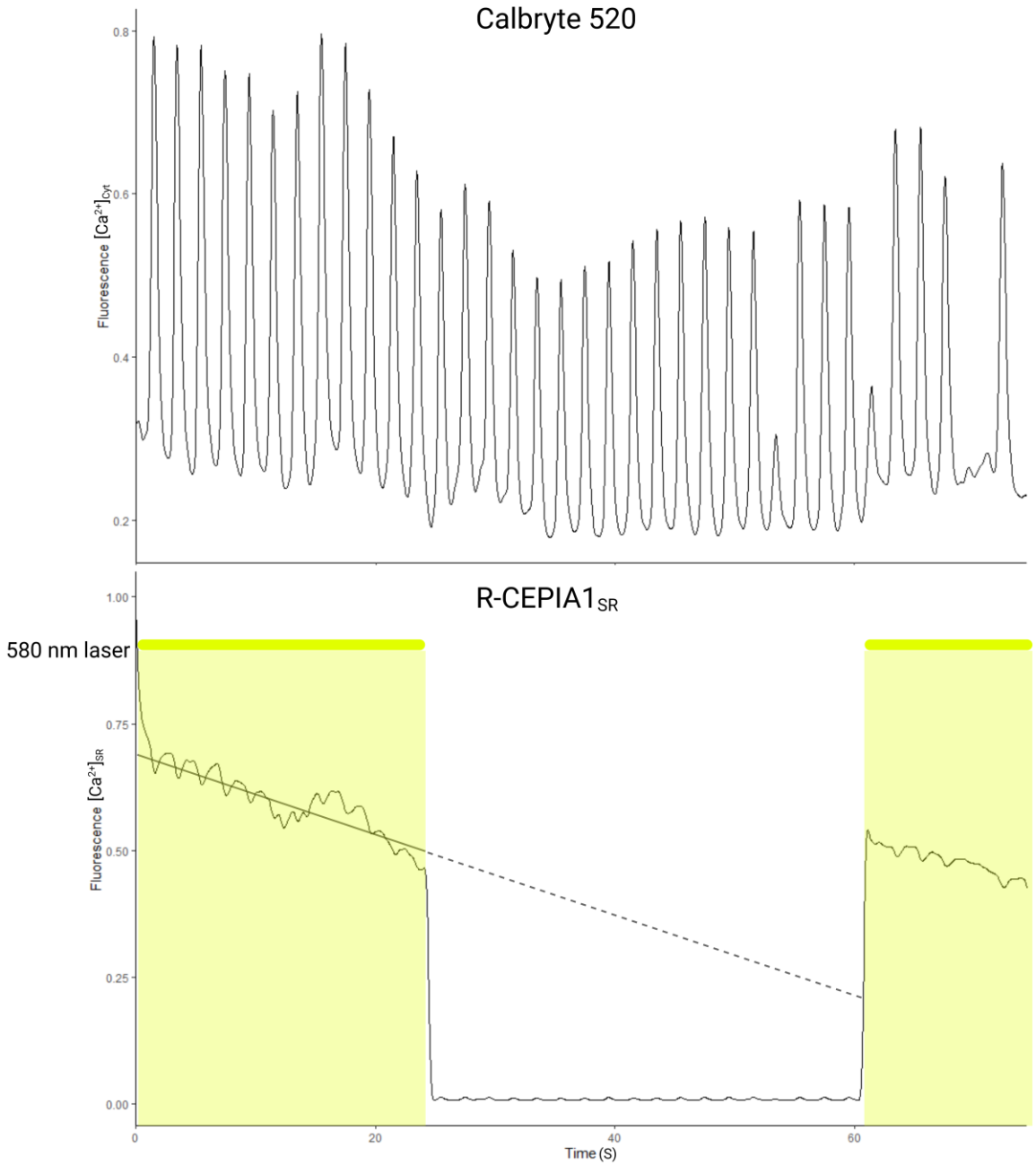

Figure 21: Fluorescence trace graphs of cytosolic and SR Ca^{2+} in R-CEPIA1$_{SR}$ expressing cells over much longer recording with intermittent darkness.

R-CEPIA1$_{SR}$ signal recovers and retains responsiveness to SR Ca^{2+} changes for over a minute given 30 seconds of darkness to recover mid-recording

Applying this mid-recording rest method to image the caffeine spike for SR Ca^{2+} depletion allows a longer imaging time window to visualize the refilling of the SR (Figure 22). Whereas previously only period immediately after the caffeine spike could be

recorded before R-CEPIA1$_{SR}$'s signal diminishes to the point of being unresponsive to SR Ca^{2+} levels, adding a rest period allows visualization of the gradually increasing SR Ca^{2+} levels throughout the process of refilling for a more accurate measurement.

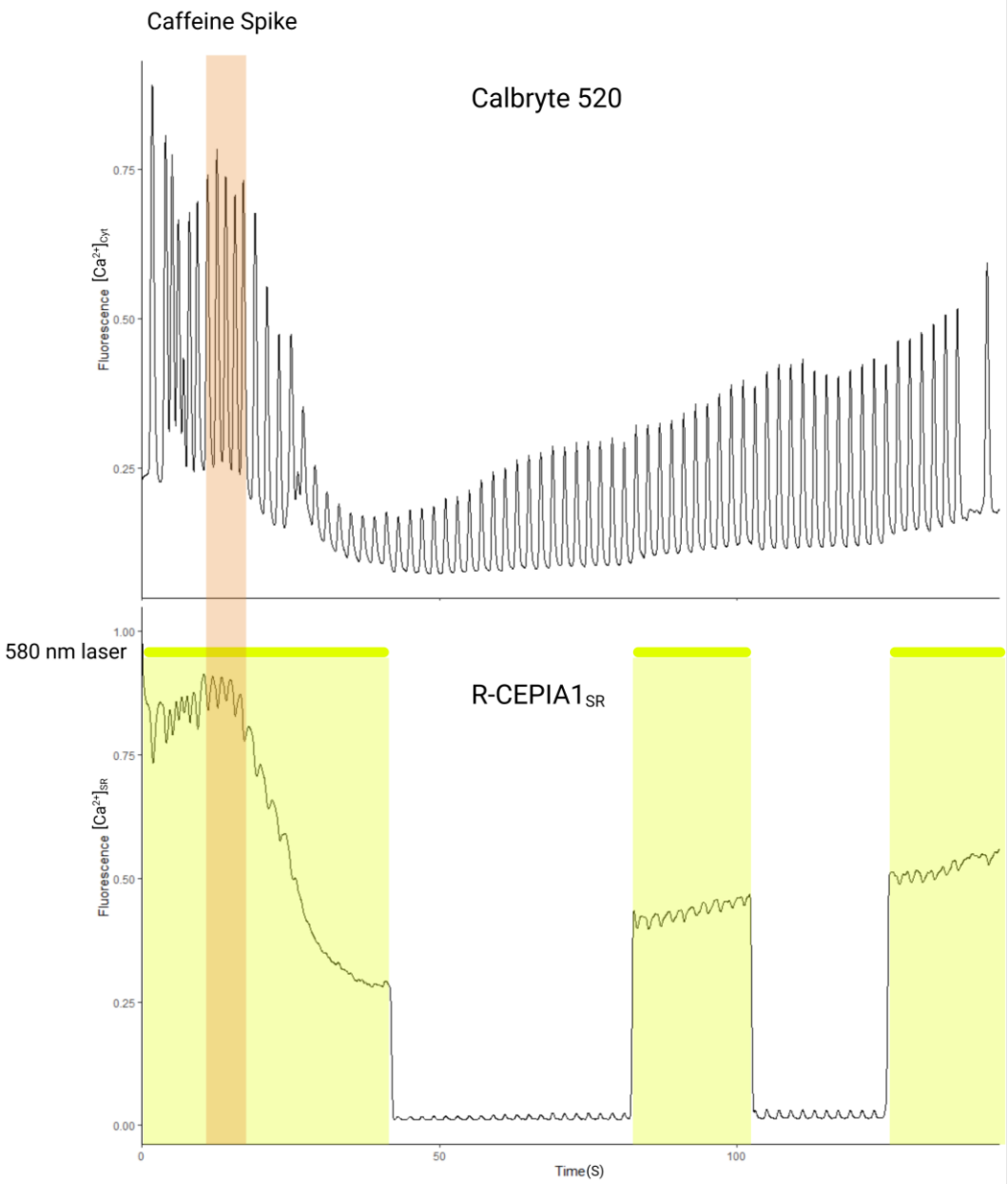

Figure 22: Fluorescence trace graphs of cytosolic and SR Ca^{2+} in R-CEPIA1$_{SR}$ expressing cells with exposure to caffeine over longer recording with intermittent darkness

Caffeine spike induces drop in SR Ca^{2+} levels followed by slow recovery of SR Ca^{2+} levels as detected by R-CEPIA1$_{SR}$ signal showing an upward slope. Longer recording over 2 minutes show that R-CEPIA1$_{SR}$ is still capable of responding to changes in SR Ca^{2+} levels if given time to recover.

G-CEPIA1$_{SR}$, the EGFP reporter replacement, was created to bypass the problem of R-CEPIA1$_{SR}$'s mApple photoswitching. Currently, G-CEPIA1$_{SR}$ has successfully been created and packaged into a lentiviral vector and is being transduced in hiPSC-CMs for imaging.

Discussion

Integration of R-CEPIA1$_{SR}$ into a genomic safe harbour site CLYBL was successful in that it showed proper integration and expression. However, the loss of the construct from the colony over time suggests that the genomic safe harbour site chosen may not be suitable for long-term expression in hiPSC-CMs. It is possible, if unlikely that contamination of wild type hiPSCs occurred, or the cell could have lost the transgene either from the genome entirely, or otherwise disabled from expressing. Therefore, antibiotic selection could be maintained to provide selective pressure for cells that have fully integrated and retained the construct, if the cell should lose it at any point. Nevertheless, for the current project, integration into CLYBL was considered not viable and instead lentiviral transduction was used as the primary expression method. Lentiviral expression is also much faster and easier to perform on new and different cell lines with different RyR2 variants, so in some ways this may have been a preferable result.

The Cl^- channel Phobos was capable of activating in response to light and allowing Cl^- through to depolarize the cells. This activation was enough to activate voltage gated ion channels, and thus to optogenetically pace the cells, however the signal was not enough to hold the membrane voltage in a depolarized state. Thus, although Phobos was functional, it did not fulfill its purpose. BLINK2 was attempted next instead of Phobos. As a K^+ channel, it is more physiologically relevant than Phobos to fill in for the lower expression of K^+ channels due to the cell's immaturity. Unfortunately, BLINK2 also does not seem to function as hoped. A likely cause for both these results could be problems in trafficking. Dr. Moroni also previously expressed concerns over whether or not BLINK2 would fully export from the ER in hiPSC-CMs. Although at the very least Phobos is confirmed to have some expression at the plasma membrane of hiPSC-CMs, a large portion of it could potentially remain trapped in the ER, effectively reducing useful expression of the construct, leading to currents too low to effectively clamp the hiPSC-CM.

Alternatively, the problem could simply be low expression levels, which can be at least partially alleviated with higher MOIs. Regrettably, as MOIs rise higher so too does toxicity and cell death, so MOIs cannot be brought too high. As both constructs are expressed simultaneously with a fluorescent reporter in the construct, the relatively low

brightness in the imaging also suggests a low expression level of the optogenetic constructs. The expression of EGFP is done through an IRES2 sequence which is known to have lower expression levels for the gene following it however, so this method could underestimate the expression levels of BLINK2. An alternative, more difficult to solve problem could be problems in trafficking to the cell surface. This can be determined with immunostaining to determine the location where the bulk of the channels eventually traffics to, however obtaining the antibody for this synthetic protein has proven difficult due to supply chain issues from the COVID pandemic. During the creation of BLINK2, other trafficking methods were also included that did improve the surface expression level such as the addition of a Kir2.1 localization sequence, however they were removed from the final product due to also causing uncontrolled activation of the channel. These trafficking signals could be added back in the event localization is found to be the main problem.

R-CEPIA1$_{SR}$ showed proper expression and localization to the SR, where it was able to report on SR Ca^{2+} levels in response to transients and drugs that modulate the SR Ca^{2+} levels. Unfortunately, the construct is very finicky and requires many adjustments to make it visible. In addition, the photoswitching property of R-CEPIA1$_{SR}$'s fluorescent reporter mApple makes longer recordings difficult. A method around this is to simply replace the fluorescent reporter with a different red fluorescent protein that does not have these properties; however circularly permuted red fluorescent proteins for use in GCaMP type constructs are very rare, and producing one ourselves would be very difficult. As an alternative to red, GFP has been previously used in GCaMP type constructs, including in the CEPIA1 type reporters. Swapping out the cpmApple for a cpGFP would be a much simpler task that can result in a much more stable SR Ca^{2+} reporter as well as less worry about crosstalk into lower wavelengths, although it may interfere with some applications that require the green wavelength for other purposes.

In conclusion, R-CEPIA1$_{SR}$ has been successfully shown to be able to be expressed in hiPSC-CMs using lentiviral transduction and is capable of reporting on SR Ca^{2+} levels simultaneously with cytosolic Ca^{2+} indicators. This will be useful as a platform for future research into the mechanisms of CPVT.

References

1. Porello ER, Mahmoud AI, Simpson E, et al. transient regenerative potential of the neonatal mouse heart. *Science (80-)*. 2011;331(Febru):1078-1080. doi:10.1126/science.1200708.Transient

2. Tsao CW, Aday AW, Almarzooq ZI, et al. *Heart Disease and Stroke Statistics-2022 Update: A Report From the American Heart Association*. Vol 145.; 2022. doi:10.1161/CIR.0000000000001052

3. Wang WE, Li L, Xia X, et al. Dedifferentiation, Proliferation, and Redifferentiation of Adult Mammalian Cardiomyocytes After Ischemic Injury. *Circulation*. 2017;136(9):834-848. doi:10.1161/CIRCULATIONAHA.116.024307

4. Clarke R. The role of preclinical animal models in breast cancer drug development. *Breast Cancer Res*. 2009;11(SUPPL. 3):11-13. doi:10.1186/bcr2441

5. Kinders R, Parchment RE, Ji J, et al. Phase 0 clinical trials in cancer drug development: From FDA guidance to clinical practice. *Mol Interv*. 2008;7(6):325-334. doi:10.1124/mi.7.6.9

6. Hingorani AD, Kuan V, Finan C, et al. Improving the odds of drug development success through human genomics: modelling study. *Sci Rep*. 2019;9(1):1-25. doi:10.1038/s41598-019-54849-w

7. Leenaars CHC, Kouwenaar C, Stafleu FR, et al. Animal to human translation: A systematic scoping review of reported concordance rates. *J Transl Med*. 2019;17(1):1-22. doi:10.1186/s12967-019-1976-2

8. Takahashi K, Yamanaka S. Induction of Pluripotent Stem Cells from Mouse Embryonic and Adult Fibroblast Cultures by Defined Factors. *Cell*. 2006. doi:10.1016/j.cell.2006.07.024

9. Giudicessi JR, Ackerman MJ. Determinants of incomplete penetrance and variable expressivity in heritable cardiac arrhythmia syndromes. *Transl Res*. 2013;161(1):1-14. doi:10.1016/j.trsl.2012.08.005

10. Jonsson MKB, Vos MA, Mirams GR, et al. Application of human stem cell-derived cardiomyocytes in safety pharmacology requires caution beyond hERG. *J Mol Cell Cardiol*. 2012;52(5):998-1008. doi:10.1016/j.yjmcc.2012.02.002

11. Ovics P, Regev D, Baskin P, et al. Drug development and the use of induced pluripotent stem cell-derived cardiomyocytes for disease modeling and drug toxicity screening. *Int J Mol Sci*. 2020;21(19):1-42. doi:10.3390/ijms21197320

12. Brown AM. Drugs, hERG and sudden death. *Cell Calcium*. 2004;35(6):543-547.

doi:10.1016/j.ceca.2004.01.008

13. Yang X, Rodriguez ML, Leonard A, et al. Fatty Acids Enhance the Maturation of Cardiomyocytes Derived from Human Pluripotent Stem Cells. *Stem Cell Reports*. 2017;9(5):1660-1674. doi:10.1016/j.stemcr.2017.10.002

14. Karbassi E, Fenix A, Marchiano S, et al. Cardiomyocyte maturation: advances in knowledge and implications for regenerative medicine. *Nat Rev Cardiol*. 2020;(Box 1). doi:10.1038/s41569-019-0331-x

15. Kadota S, Pabon L, Reinecke H, Murry CE. In Vivo Maturation of Human Induced Pluripotent Stem Cell-Derived Cardiomyocytes in Neonatal and Adult Rat Hearts. *Stem Cell Reports*. 2017;8(2):278-289. doi:10.1016/j.stemcr.2016.10.009

16. Guo Y, Pu WT. Cardiomyocyte maturation: New phase in development. *Circ Res*. 2020:1086-1106. doi:10.1161/CIRCRESAHA.119.315862

17. Herron TJ, Da Rocha AM, Campbell KF, et al. Extracellular matrix-mediated maturation of human pluripotent stem cell-derived cardiac monolayer structure and electrophysiological function. *Circ Arrhythmia Electrophysiol*. 2016;9(4):1-12. doi:10.1161/CIRCEP.113.003638

18. Rasmussen H, Barrett PQ. Calcium messenger system: An integrated view. *Physiol Rev*. 1984;64(3):938-984. doi:10.1152/physrev.1984.64.3.938

19. Beard NA, Laver DR, Dulhunty AF. Calsequestrin and the calcium release channel of skeletal and cardiac muscle. *Prog Biophys Mol Biol*. 2004;85(1):33-69. doi:10.1016/j.pbiomolbio.2003.07.001

20. Shannon TR, Guo T, Bers DM. Ca2+ scraps local depletions of free [Ca2+] in cardiac sarcoplasmic reticulum during contractions leave substantial Ca2+ reserve. *Circ Res*. 2003;93(1):40-45. doi:10.1161/01.RES.0000079967.11815.19

21. Lanner JT, Georgiou DK, Joshi AD, Hamilton SL. Ryanodine Receptors: Structure, Expression, Molecular Details, and Function in Calcium Release. *Cold Spring Harb Perspect Biol*. 2010;2(11):a003996-a003996. doi:10.1101/cshperspect.a003996

22. Jiang D, Xiao B, Yang D, et al. RyR2 mutations linked to ventricular tachycardia and sudden death reduce the threshold for store-overload-induced Ca2+ release (SOICR). *Proc Natl Acad Sci U S A*. 2004;101(35):13062-13067. doi:10.1073/pnas.0402388101

23. Roston TM, Van Petegem F, Sanatani S. Catecholaminergic polymorphic ventricular tachycardia: A model for genotype-specific therapy. *Curr Opin Cardiol*. 2017;32(1):78-85. doi:10.1097/HCO.0000000000000360

24. Preininger MK, Jha R, Maxwell JT, et al. RESEARCH ARTICLE A human

pluripotent stem cell model of catecholaminergic polymorphic ventricular tachycardia recapitulates patient-specific drug responses. 2016:927-939. doi:10.1242/dmm.026823

25. Wleklinski MJ, Kannankeril PJ, Knollmann BC. Molecular and tissue mechanisms of catecholaminergic polymorphic ventricular tachycardia. *J Physiol*. 2020;598(14):2817-2834. doi:10.1113/JP276757

26. Cheng H, Lederer WJ. Calcium sparks. *Physiol Rev*. 2008;88(4):1491-1545. doi:10.1152/physrev.00030.2007

27. SOBIE E, GUATIMOSIM S, GOMEZVIQUEZ L, et al. The Ca2+ leak paradox and “rogue ryanodine receptors”: SR Ca2+ efflux theory and practice. *Prog Biophys Mol Biol*. 2006;90(1-3):172-185. doi:10.1016/j.pbiomolbio.2005.06.010

28. Guo T, Gillespie D, Fill M. Ryanodine Receptor Current Amplitude Controls Ca 2+ Sparks in Cardiac Muscle. *Circ Res*. 2012;111(1):28-36. doi:10.1161/CIRCRESAHA.112.265652

29. Zahradníková A, Valent I, Zahradník I. Frequency and release flux of calcium sparks in rat cardiac myocytes: A relation to RYR gating. *J Gen Physiol*. 2010;136(1):101-116. doi:10.1085/jgp.200910380

30. Kushnir A, Marx SO. *Voltage-Gated Calcium Channels*. Seventh Ed. Elsevier Inc.; 2018. doi:10.1016/B978-0-323-44733-1.00002-X

31. Babai N, Kanevsky N, Dascal N, et al. Anion-sensitive regions of L-type CaV1.2 calcium channels expressed in HEK293 cells. *PLoS One*. 2010;5(1). doi:10.1371/journal.pone.0008602

32. Laksman Z, Wauchop M, Lin E, et al. Modeling Atrial Fibrillation using Human Embryonic Stem Cell-Derived Atrial Tissue. *Sci Rep*. 2017;7(1):1-11. doi:10.1038/s41598-017-05652-y

33. Zhang Z, Zhao Z, Liu Y, Wang W, Wu Y, Ding J. Kinetic Model of Nav1.5 Channel Provides a Subtle Insight into Slow Inactivation Associated Excitability in Cardiac Cells. *PLoS One*. 2013;8(5). doi:10.1371/journal.pone.0064286

34. Bers DM. Calcium cycling and signaling in cardiac myocytes. *Annu Rev Physiol*. 2008;70:23-49. doi:10.1146/annurev.physiol.70.113006.100455

35. Devalla HD, Gélinas R, Aburawi EH, et al. TECRL , a new life- threatening inherited arrhythmia gene associated with overlapping clinical features of both LQTS and CPVT . *EMBO Mol Med*. 2016;8(12):1390-1408. doi:10.15252/emmm.201505719

36. Pérez-Riera AR, Barbosa-Barros R, de Rezende Barbosa MPC, Daminello-Raimundo R, de Lucca AA, de Abreu LC. Catecholaminergic polymorphic

ventricular tachycardia, an update. *Ann Noninvasive Electrocardiol*. 2018;23(4):1-10. doi:10.1111/anec.12512

37. Kimlicka L, Lau K, Tung CC, Van Petegem F. Disease mutations in the ryanodine receptor N-terminal region couple to a mobile intersubunit interface. *Nat Commun*. 2013;4:1506-1510. doi:10.1038/ncomms2501

38. Meli AC, Refaat MM, Dura M, et al. A Novel Ryanodine Receptor Mutation Linked to Sudden Death Increases Sensitivity to Cytosolic Calcium. *Circ Res*. 2011;109(3):281-290. doi:10.1161/CIRCRESAHA.111.244970

39. Jiang D, Wang R, Xiao B, et al. Enhanced store overload-induced Ca2+ release and channel sensitivity to luminal Ca2+ activation are common defects of RyR2 mutations linked to ventricular tachycardia and sudden death. *Circ Res*. 2005;97(11):1173-1181. doi:10.1161/01.RES.0000192146.85173.4b

40. Lobo PA, Kimlicka L, Tung CC, Van Petegem F. The deletion of exon 3 in the cardiac ryanodine receptor is rescued by β strand switching. *Structure*. 2011;19(6):790-798. doi:10.1016/j.str.2011.03.016

41. Shannon TR, Ginsburg KS, Bers DM. Quantitative assessment of the SR Ca 2+ leak-load relationship. *Circ Res*. 2002;91(7):594-600. doi:10.1161/01.RES.0000036914.12686.28

42. Bai Y, Jones PP, Guo J, et al. Phospholamban Knockout Breaks Arrhythmogenic Ca 2+ Waves and Suppresses Catecholaminergic Polymorphic Ventricular Tachycardia in Mice. *Circ Res*. 2013;113(5):517-526. doi:10.1161/CIRCRESAHA.113.301678

43. Tsukamoto S, Fujii T, Oyama K, et al. Simultaneous imaging of local calcium and single sarcomere length in rat neonatal cardiomyocytes using yellow Cameleon-Nano140. *J Gen Physiol*. 2016;148(4):341-355. doi:10.1085/jgp.201611604

44. Tiburcy M, Hudson JE, Balfanz P, et al. Defined engineered human myocardium with advanced maturation for applications in heart failure modeling and repair. *Circulation*. 2017;135(19):1832-1847. doi:10.1161/CIRCULATIONAHA.116.024145

45. Madamanchi A. B-Adrenergic Receptor Signaling in Cardiac Function and Heart Failure. *McGill J Med*. 2007;10(2):99-104. doi:10.26443/mjm.v10i2.458

46. Grimm M, Brown JH. β-Adrenergic receptor signaling in the heart: Role of CaMKII. *J Mol Cell Cardiol*. 2010;48(2):322-330. doi:10.1016/j.yjmcc.2009.10.016

47. Liu N, Rizzi N, Boveri L, Priori SG. Ryanodine receptor and calsequestrin in arrhythmogenesis: What we have learnt from genetic diseases and transgenic mice. *J Mol Cell Cardiol*. 2009;46(2):149-159. doi:10.1016/j.yjmcc.2008.10.012

48. Mattiazzi A, Mundiña-Weilenmann C, Guoxiang C, Vittone L, Kranias E. Role of phospholamban phosphorylation on Thr17 in cardiac physiological and pathological conditions. *Cardiovasc Res*. 2005;68(3):366-375. doi:10.1016/j.cardiores.2005.08.010

49. Baier MJ, Noack J, Seitz MT, Maier LS, Neef S. Phosphorylation of RyR2 Ser-2814 by CaMKII mediates β1-adrenergic stress induced Ca2+-leak from the sarcoplasmic reticulum. *FEBS Open Bio*. 2021;11(10):2756-2762. doi:10.1002/2211-5463.13274

50. Uchinoumi H, Yang Y, Oda T, et al. CaMKII-dependent phosphorylation of RyR2 promotes targetable pathological RyR2 conformational shift. *J Mol Cell Cardiol*. 2016;98(4):62-72. doi:10.1016/j.yjmcc.2016.06.007

51. MacLennan DH, Chen SRW. Store overload-induced Ca2+ release as a triggering mechanism for CPVT and MH episodes caused by mutations in RYR and CASQ genes. *J Physiol*. 2009;587(13):3113-3115. doi:10.1113/jphysiol.2009.172155

52. Xiao Z, Guo W, Sun B, et al. Enhanced cytosolic Ca2+activation underlies a common defect of central domain cardiac ryanodine receptor mutations linked to arrhythmias. *J Biol Chem*. 2016;291(47):24528-24537. doi:10.1074/jbc.M116.756528

53. Márquez MF, Totomoch-Serra A, Rueda A, Avelino-Cruz JE, Gallegos-Cortez A. Basic and clinical insights in catecholaminergic (familial) polymorphic ventricular tachycardia. *Rev Investig Clin*. 2019;71(4):226-236. doi:10.24875/RIC.19002939

54. Rosso R, Kalman JM, Rogowski O, et al. Calcium channel blockers and beta-blockers versus beta-blockers alone for preventing exercise-induced arrhythmias in catecholaminergic polymorphic ventricular tachycardia. *Hear Rhythm*. 2007;4(9):1149-1154. doi:10.1016/j.hrthm.2007.05.017

55. Bannister ML, Thomas NL, Sikkel MB, et al. The mechanism of flecainide action in CPVT does not involve a direct effect on RyR2. *Circ Res*. 2015;116(8):1324-1335. doi:10.1161/CIRCRESAHA.116.305347

56. Bansal R, Mahajan A, Vichare S, Lokhandwala Y. Cardiac sympathetic denervation for catecholaminergic polymorphic ventricular tachycardia. *J Postgrad Med*. 2008;68(1):41-43. doi:10.4103/jpgm.JPGM_908_20

57. Palmer AE, Tsien RY. Measuring calcium signaling using genetically targetable fluorescent indicators. *Nat Protoc*. 2006;1(3):1057-1065. doi:10.1038/nprot.2006.172

58. Inoue M, Takeuchi A, Manita S, et al. Rational Engineering of XCaMPs, a Multicolor GECI Suite for In Vivo Imaging of Complex Brain Circuit Dynamics. *Cell*. 2019;177(5):1346-1360.e24. doi:10.1016/j.cell.2019.04.007

59. Mollinedo-Gajate I, Song C, Knöpfel T. Genetically encoded fluorescent calcium

and voltage indicators. *Handb Exp Pharmacol*. 2019;260:209-229. doi:10.1007/164_2019_299

60. Kostyuk AI, Demidovich AD, Kotova DA, Belousov V V., Bilan DS. Circularly permuted fluorescent protein-based indicators: History, principles, and classification. *Int J Mol Sci*. 2019;20(17). doi:10.3390/ijms20174200

61. Zhou X, Belavek KJ, Miller EW. Origins of Ca 2+ Imaging with Fluorescent Indicators. 2021;(Figure 1). doi:10.1021/acs.biochem.1c00350

62. Zhang D, Redington E, Gong Y. Rational engineering of ratiometric calcium sensors with bright green and red fluorescent proteins. *Commun Biol*. 2021;4(1):1-12. doi:10.1038/s42003-021-02452-z

63. Shaner NC, Lin MZ, McKeown MR, et al. Improving the photostability of bright monomeric orange and red fluorescent proteins. *Nat Methods*. 2008;5(6):545-551. doi:10.1038/nmeth.1209

64. Akerboom J, Calderón NC, Tian L, et al. Genetically encoded calcium indicators for multi-color neural activity imaging and combination with optogenetics. *Front Mol Neurosci*. 2013;(FEB). doi:10.3389/fnmol.2013.00002

65. Bindels DS, Haarbosch L, Van Weeren L, et al. MScarlet: A bright monomeric red fluorescent protein for cellular imaging. *Nat Methods*. 2016;14(1):53-56. doi:10.1038/nmeth.4074

66. Samtleben S, Jaepel J, Fecher C, Andreska T, Rehberg M, Blum R. Direct imaging of ER calcium with targeted-esterase induced dye loading (TED). *J Vis Exp*. 2013;(75):1-17. doi:10.3791/50317

67. Blum R, Petersen OH, Verkhratsky A. Ca2+ Imaging of Intracellular Organelles: Endoplasmic Reticulum. In: ; 2010:147-167. doi:10.1007/978-1-60761-476-0_8

68. Ryu M, Moskvin O V, Siltberg-liberles J, Gomelsky M. Natural and Engineered Photoactivated Nucleotidyl Cyclases for Optogenetic Applications. 2010;285(53):41501-41508. doi:10.1074/jbc.M110.177600

69. Kato HE, Zhang F, Yizhar O, et al. Crystal structure of the channelrhodopsin light-gated cation channel. 2012. doi:10.1038/nature10870

70. Kopton RA, Baillie JS, Rafferty SA, et al. Cardiac Electrophysiological Effects of Light-Activated Chloride Channels. *Front Physiol*. 2018;9(December):1806. doi:10.3389/FPHYS.2018.01806

71. Zhang F, Vierock J, Yizhar O, et al. The microbial opsin family of optogenetic tools. *Cell*. 2011;147(7):1446-1457. doi:10.1016/j.cell.2011.12.004

72. Gradinaru V, Zhang F, Ramakrishnan C, et al. Molecular and Cellular Approaches

for Diversifying and Extending Optogenetics. *Cell*. 2010;141(1):154-165. doi:10.1016/j.cell.2010.02.037

73. Ehrlich JR, Cha TJ, Zhang L, et al. Characterization of a hyperpolarization-activated time-dependent potassium current in canine cardiomyocytes from pulmonary vein myocardial sleeves and left atrium. *J Physiol*. 2004;557(2):583-597. doi:10.1113/jphysiol.2004.061119

74. Bett GCL, Kaplan AD, Lis A, et al. Electronic “expression” of the inward rectifier in cardiocytes derived from human-induced pluripotent stem cells. *Hear Rhythm*. 2013;10(12):1903-1910. doi:10.1016/j.hrthm.2013.09.061

75. Alberio L, Locarno A, Saponaro A, et al. A light-gated potassium channel for sustained neuronal inhibition. *Nat Methods*. 2018;15(11):969-976. doi:10.1038/s41592-018-0186-9

76. Pagliuca C, Goetze TA, Wagner R, Thiel G, Moroni A, Parcej D. Molecular properties of Kcv, a virus encoded K+ channel. *Biochemistry*. 2007;46(4):1079-1090. doi:10.1021/bi061530w

77. Christie JM, Gawthorne J, Young G, Fraser NJ, Roe AJ. LOV to BLUF: Flavoprotein contributions to the optogenetic toolkit. *Mol Plant*. 2012;5(3):533-544. doi:10.1093/mp/sss020

78. Christie JM. Phototropin blue-light receptors. *Annu Rev Plant Biol*. 2007;58:21-45. doi:10.1146/annurev.arplant.58.032806.103951

79. Wietek J, Rodriguez-Rozada S, Tutas J, et al. Anion-conducting channelrhodopsins with tuned spectra and modified kinetics engineered for optogenetic manipulation of behavior. *Sci Rep*. 2017;7(1):1-18. doi:10.1038/s41598-017-14330-y

80. Hansen TH, Yan Y, Ahlberg G, et al. A Novel Loss-of-Function Variant in the Chloride Ion Channel Gene Clcn2 Associates with Atrial Fibrillation. *Sci Rep*. 2020;10(1):1-10. doi:10.1038/s41598-020-58475-9

81. Vigna E, Naldini L. Lentiviral vectors: Excellent tools for experimental gene transfer and promising candidates for gene therapy. *J Gene Med*. 2000;2(5):308-316. doi:10.1002/1521-2254(200009/10)2:5<308::aid-jgm131>3.0.co;2-3

82. Gallay P, Hope T, Chin D, Trono D. HIV-1 infection of nondividing cells through the recognition of integrase by the importin/karyopherin pathway. *Proc Natl Acad Sci U S A*. 1997;94(18):9825-9830. doi:10.1073/pnas.94.18.9825

83. Oceguera-yanez F, Kim S, Matsumoto T, et al. Engineering the AAVS1 locus for consistent and scalable transgene expression in human iPSCs and their differentiated derivatives. *Methods*. 2016;101:43-55. doi:10.1016/j.ymeth.2015.12.012

84. Kotin RM, Linden RM, Berns KI. Characterization of a preferred site on human chromosome 19q for integration of adeno-associated virus DNA by non-homologous recombination. *EMBO J*. 1992;11(13):5071-5078. doi:10.1002/j.1460-2075.1992.tb05614.x

85. Deyle DR, Russell DW. Adeno-associated virus vector integration. *Curr Opin Mol Ther*. 2009;11(4):442-447. http://www.pubmedcentral.nih.gov/articlerender.fcgi?artid=2929125&tool=pmcentrez&rendertype=abstract.

86. Dutheil N, Shi F, Dupressoir T, Linden RM. Adeno-associated virus site-specifically integrates into a muscle-specific DNA region. *Proc Natl Acad Sci U S A*. 2000;97(9):4862-4866. doi:10.1073/pnas.080079397

87. Weltner J, Anisimov A, Alitalo K, Otonkoski T, Trokovic R. Induced Pluripotent Stem Cell Clones Reprogrammed via Recombinant Adeno-Associated Virus-Mediated Transduction Contain Integrated Vector Sequences. *J Virol*. 2012;86(8):4463-4467. doi:10.1128/jvi.06302-11

88. Sun Y, Kao HKJ, Merleev CCA, Chiamvimonvat N, Chan JW. Human induced pluripotent stem cell line with genetically encoded fluorescent voltage indicator generated via CRISPR for action potential assessment post-cardiogenesis. doi:10.1002/stem.3085

89. Klatt D, Cheng E, Hoffmann Di, et al. Differential Transgene Silencing of Myeloid-Specific Promoters in the AAVS1 Safe Harbor Locus of Induced Pluripotent Stem Cell-Derived Myeloid Cells. *Hum Gene Ther*. 2020;31(3-4):199-210. doi:10.1089/hum.2019.194

90. Cerbini T, Funahashi R, Luo Y, et al. Transcription activator-like effector nuclease (TALEN)-mediated CLYBL targeting enables enhanced transgene expression and one-step generation of dual reporter human induced pluripotent stem cell (iPSC) and neural stem cell (NSC) lines. *PLoS One*. 2015;10(1):1-18. doi:10.1371/journal.pone.0116032

91. Lian X, Zhang J, Azarin S, et al. Directed cardiomyocyte differentiation from human pluripotent ste cells by modulating Wnt/beta-catenin signaling under fully defined conditions. *Nat Protoc*. 2013;8(1):162-175. doi:10.1038/nprot.2012.150.Directed

92. Sharma A, Li G, Rajarajan K, Hamaguchi R, Burridge PW, Wu SM. Derivation of highly purified cardiomyocytes from human induced pluripotent stem cells using small molecule-modulated differentiation and subsequent glucose starvation. *J Vis Exp*. 2015;2015(97):3-10. doi:10.3791/52628

93. Suzuki J, Kanemaru K, Ishii K, Ohkura M, Okubo Y, Iino M. Imaging intraorganellar Ca2+at subcellular resolution using CEPIA. *Nat Commun*. 2014;5(May):1-13. doi:10.1038/ncomms5153

94. Nakai J, Ohkura M, Imoto K. A high signal-to-noise Ca2+ probe composed of a single green fluorescent protein. *Nat Biotechnol*. 2001;19(2):137-141. doi:10.1038/84397

95. Zhao Y, Araki S, Wu J, et al. An Expanded Palette of Genetically Encoded Ca2+ Indicators. *Science (80-)*. 2011;333(6051):1888-1891. doi:10.1126/science.1208592

96. Romani G, Piotrowski A, Hillmer S, et al. A virus-encoded potassium ion channel is a structural protein in the chlorovirus Paramecium bursaria chlorella virus 1 virion. *J Gen Virol*. 2013;94(PART 11):2549-2556. doi:10.1099/vir.0.055251-0

97. Swartz TE, Corchnoy SB, Christie JM, et al. The Photocycle of a Flavin-binding Domain of the Blue Light Photoreceptor Phototropin. *J Biol Chem*. 2001;276(39):36493-36500. doi:10.1074/jbc.M103114200

98. Moriya K, Nagatoshi K, Noriyasu Y, et al. Protein N-myristoylation plays a critical role in the endoplasmic reticulum morphological change induced by overexpression of protein lunapark, an integral membrane protein of the endoplasmic reticulum. *PLoS One*. 2013;8(11). doi:10.1371/journal.pone.0078235

99. McIlhinney RAJ. Membrane Targeting via Protein N-Myristoylation. In: *Protein Targeting Protocols*. Vol 53. New Jersey: Humana Press; 1998:211-226. doi:10.1385/0-89603-487-9:211

100. Sottocornola B, Visconti S, Orsi S, et al. The potassium channel KAT1 is activated by plant and animal 14-3-3 proteins. *J Biol Chem*. 2006;281(47):35735-35741. doi:10.1074/jbc.M603361200

101. Arslanova A, Shafaattalab S, Ye K, et al. Using hiPSC-CMs to Examine Mechanisms of Catecholaminergic Polymorphic Ventricular Tachycardia. *Curr Protoc*. 2021;1(12). doi:10.1002/cpz1.320